A biased adenosine A_1R agonist confers analgesia without cardiorespiratory depression

Mark J. Wall[1*], Emily Hill[1], Robert Huckstepp[1], Kerry Barkan[2], Giuseppe Deganutti[3,♦], Michele Leuenberger[4], Barbara Preti[4], Ian Winfield[2], Haifeng Wei[5], Wendy Imlach[6], Eve Dean[1], Cherise Hume[1], Stephanie Hayward[1], Jess Oliver[1], Fei-Yue Zhao[5], David Spanswick[5,6,7], Christopher A. Reynolds[3,♦], Martin Lochner[4], Graham Ladds[2] and Bruno G. Frenguelli[1]

*Author for correspondence

[1]School of Life Sciences

University of Warwick

Gibbet Hill Rd

Coventry CV4 7AL, UK

[2]Department of Pharmacology

University of Cambridge

Tennis Court Road

Cambridge CB2 1PD, UK

[3]School of Biological Sciences

University of Essex

Wivenhoe Park

Colchester CO4 3SQ, UK

[4]Institute of Biochemistry and Molecular Medicine

University of Bern

3012 Bern, Switzerland

[5]NeuroSolutions Ltd, Coventry, UK.

[6]Department of Physiology

Monash Biomedicine Discovery Institute

Monash University

Innovation Walk

Clayton VIC 3800, Australia

[7]Warwick Medical School

University of Warwick

Gibbet Hill Rd

Coventry CV4 7AL, UK

♦Current Address:

Centre for Sport, Exercise and Life Sciences (CSELS),

Faculty of Health and Life Sciences,

Coventry University,

Coventry CV1 2DS, UK

Summary

The development of therapeutic agonists for G protein-coupled receptors (GPCRs) is hampered by the propensity of GPCRs to couple to multiple Gα subunits. This promiscuous coupling leads to numerous downstream cellular effects, some of which are therapeutically undesirable. This is especially the case for adenosine A_1 receptors (A_1Rs) whose clinical potential is undermined by the sedation and cardiorespiratory depression caused by conventional agonists. We have discovered that the A_1R-selective agonist, BnOCPA, is a potent and powerful analgesic but does not cause sedation, bradycardia, hypotension or respiratory depression. This unprecedented discrimination between native A_1Rs arises from BnOCPA's unique and highly biased activation of Gob among the six Gαi/o subtypes, and in the absence of β-arrestin recruitment. BnOCPA thus demonstrates a hitherto unknown Gα-selective activation of the native A_1R, sheds new light on the fundamentals of GPCR signalling, and reveals new possibilities for the development of novel therapeutics based on the far-reaching concept of biased agonism.

Abbreviated summary:

We describe the selective activation of an adenosine A_1 receptor-mediated intracellular pathway that provides potent analgesia in the absence of sedation or cardiorespiratory depression, paving the way for novel medicines based on the far-reaching concept of biased agonism.

Introduction

G protein-coupled receptors (GPCRs) are the targets of many FDA-approved drugs (Congreve et al., 2020; Hauser et al., 2017). However, the promiscuity with which they couple to multiple intracellular signalling cascades leads to unwanted side effects. These side effects limit both the range of GPCRs suitable for drug-targeting, and the number of conditions for which treatments could be developed (Kenakin, 2018; Michel and Charlton, 2018). One family of GPCRs that has particularly suffered as drug targets from their promiscuous coupling are the four GPCRs for the purine nucleoside adenosine, despite the potential for using adenosine receptor agonists to treat many pathological conditions including cancer, cardiovascular, neurological and inflammatory diseases (Borea et al., 2018; Jacobson and Muller, 2016; Sawynok, 2016). For example, activation of the widely-distributed adenosine A_1 receptor (A_1R) with currently available agonists elicits multiple actions in both the central nervous system (CNS), such as the inhibition of synaptic transmission, neuronal hyperpolarization, and sedation, and in the cardiorespiratory system through slowing the heart (bradycardia), reducing blood pressure (hypotension), and depressing respiration (dyspnea) (Dunwiddie and Masino, 2001; Headrick et al., 2013; Sawynok, 2016; Vecchio et al., 2018). These multiple effects severely limit the prospects of A_1R agonists as life-changing medicines, despite their potential use in a wide range of clinical conditions including glaucoma, type 2 diabetes mellitus, pain, epilepsy and cerebral ischemia (Baltos et al., 2016; Deb et al., 2019; Sawynok, 2016; Varani et al., 2017; Weltha et al., 2018).

The therapeutic limitations of promiscuous GPCR coupling might be overcome through the development of biased agonists – compounds that selectively recruit one intracellular signalling cascade over another (Kenakin, 2019; Michel and Charlton, 2018; Wootten et al., 2018). This signalling bias has most frequently been expressed in terms of Gα vs β-arrestin signalling (Violin and Lefkowitz, 2007) and has been pursued in the treatment of drug addiction (Slosky et al., 2020), and in the context of opioid receptor agonists producing analgesia with reduced respiratory depression (Michel and Charlton, 2018), but not without controversy (Kliewer et al., 2020). However, while other forms of bias exist, including between individual Gα subunits (Kenakin, 2019), the challenge remains in translating Gα signalling bias observed *in vitro* to tangible, and physiologically-

relevant, selectivity at native receptors *in vivo* (Kenakin, 2018; Michel and Charlton, 2018). Accordingly, while the potential to selectively drive the G protein-coupling of A_1Rs has been described in several *in vitro* studies (Aurelio et al., 2018; Cordeaux et al., 2004; Stewart et al., 2009; Valant et al., 2014), to date no A_1R-specific agonist has been reported that can elicit Gα biased agonism at native A_1Rs in intact physiological systems. To do so would introduce novel therapeutic opportunities across a wide range of debilitating clinical conditions.

Utilising molecular dynamics simulations and Gαi/o subunit-specific cellular signalling assays we describe how one A_1R-selective agonist, BnOCPA (Knight et al., 2016), fulfils the criteria for a biased agonist in exclusively activating Gob among the six members of the Gαi/o family of G protein subunits, and in the absence of β-arrestin recruitment. In addition, through a combination of CNS electrophysiology, physiological recordings of cardiorespiratory parameters and the use of a clinically-relevant model of chronic neuropathic pain, we demonstrate selective activation of native A_1Rs and the delivery of potent analgesia without sedation, motor impairment or cardiorespiratory depression. Our data thus demonstrate the translation of agonist bias *in vitro* to therapeutically-tangible clinically-relevant observations *in vivo*. Such observations reveal the possibility of achieving agonist bias at native receptors, highlight the physiological benefits of such bias, and specifically speak to the possibility of unlocking the widespread clinical potential of A_1R agonists.

RESULTS

The novel A_1R agonist BnOCPA uniquely discriminates between pre- and postsynaptic actions of native A_1Rs in the intact mammalian CNS.

BnOCPA (Figure 1A) is a cyclopentyl derivative of adenosine and a highly selective and potent, full agonist at human adenosine A_1Rs (hA_1Rs; Figure 1B; Table S1). It binds to the receptor with an affinity equal to that of prototypical A_1R agonists CPA and NECA, and higher than that of the endogenous agonist adenosine (Figure 1B; Table S1). These initial pharmacological studies at recombinant hA_1Rs in cell lines did not reveal anything extraordinary about BnOCPA. However, when we investigated BnOCPA at native A_1Rs in rat hippocampal slices, against which BnOCPA is also a potent agonist with a 15-fold selectivity against A_2A and A_3Rs (Table S2), we discovered properties of BnOCPA that were not consistent with those of typical A_1R agonists such as adenosine, CPA and NECA. In accordance with the effects of standard A_1R agonists, BnOCPA potently inhibited excitatory synaptic transmission in rat hippocampal slices (IC_{50} ~65 nM; Figure 1C to G and Figure S1A to D), an effect attributable to activation of native presynaptic A_1Rs on glutamatergic terminals (Dunwiddie and Masino, 2001) (Figure 1C; Figure S1E, F). However, in stark contrast to adenosine and CPA, BnOCPA did not activate postsynaptic A_1Rs (Figure 1C) to induce membrane hyperpolarisation, even at concentrations 15 times the IC_{50} for the inhibition of synaptic transmission (Figure 1H, I).

This peculiar and unprecedented discrimination between pre- and postsynaptic A_1Rs might possibly be explained in terms of some hindrance in the binding of BnOCPA to A_1Rs on postsynaptic neurones. To determine whether BnOCPA actually bound to postsynaptic A_1Rs, but without efficacy, we reasoned that BnOCPA might behave in a manner analogous to a receptor antagonist in preventing or reversing activation by other A_1R agonists, a property that has been predicted and observed for biased agonists at other receptors (Kenakin, 2019). To test this, we pre-applied BnOCPA then applied CPA (in the continued presence of BnOCPA). Remarkably, the co-application of CPA and BnOCPA resulted in a significant reduction of the effects of CPA on membrane potential (Figure 1I; Figure S2A, B). In addition, membrane hyperpolarisation induced by the endogenous

agonist adenosine was reversed by BnOCPA (Figure S2C). To test whether this was a trivial action of BnOCPA in blocking K^+ channels mediating the postsynaptic hyperpolarisation, or in some other way non-specifically interfering with G protein signalling, we applied the $GABA_B$ receptor agonist baclofen to CA1 pyramidal neurons. BnOCPA had no effect on membrane hyperpolarisation produced by baclofen (Figure S2D, E), confirming that the actions of BnOCPA were specific to the A_1R. These observations, of a lack of effect of BnOCPA on postsynaptic membrane potential, likely explained why, in a model of seizure activity with prominent postsynaptic depolarisation that promotes neuronal firing, (low Mg^{2+}/high K^+), BnOCPA had little effect (Figure 1J, K). In contrast, equivalent concentrations of CPA completely suppressed neuronal firing (Figure 1J, K).

BnOCPA demonstrates unique Gα signalling bias in the selective activation of Gob.

The observation that BnOCPA discriminates between pre- and postsynaptic A_1Rs might be explained if these receptors were to activate different Gαi/o proteins to mediate their effects, and that BnOCPA was not able to activate the A_1R-Gαi/o complex responsible for postsynaptic membrane hyperpolarisation. To investigate whether BnOCPA has the ability to discriminate among the various Gαi/o subunits activated by adenosine, we generated a recombinant cell system (CHO-K1 cells) expressing both the hA_1R and individual pertussis toxin (PTX)-insensitive variants of individual Gαi/o subunits. In cells treated with PTX to inhibit endogenous Gαi/o (Knight et al., 2016; Stewart et al., 2009) we observed that adenosine, CPA, NECA and the novel unbiased agonist HOCPA (Knight et al., 2016) activated a range of Gαi/o subunits, including both Gαo isoforms, Goa and Gob (Figure 2A, B; Table 1; Table S1; Figures S3 & S4). Such promiscuous Gα coupling has been described previously for adenosine, CPA, and NECA at recombinant A_1Rs in cell lines (Avet et al., 2020; Cordeaux et al., 2004; Wise et al., 1999). In stark contrast, BnOCPA displayed a unique and highly distinctive Gαi/o subunit activation profile: BnOCPA was not able to activate Gi1, Gi2, Gi3 or Gz, and was furthermore capable of discriminating between the two Gαo isoforms via the selective activation of Gob, and not of Goa (Figure 2A, B; Table 1; Figure S3).

We excluded the possibility that the actions of BnOCPA and the prototypical A_1R agonists were mediated via β-arrestins using a BRET assay for β-arrestin recruitment (Figure S5). We observed no β-arrestin recruitment at the A_1R using either BnOCPA, CPA or adenosine (Figure S5), observations that are consistent with those previously reported for recombinant A_1Rs expressing native sequences (Ciruela et al., 1997; Escriche et al., 2003; Ferguson et al., 2002; Gines et al., 2001; Iacovelli et al., 1999). The lack of β-arrestin recruitment is likely due to the lack of serine and threonine residues in the A_1R cytoplasmic tail, which makes the A_1R intrinsically biased against β-arrestin signalling (Violin and Lefkowitz, 2007; Yin et al., 2019).

The selective and unique biased activation of Gob among the six Gαi/o subunits by BnOCPA can be observed in a comparison of the activation of Goa and Gob by the A_1R agonists in their ability to inhibit the forskolin-stimulated accumulation of cAMP (Figure 2C). Whereas adenosine, CPA, NECA and HOCPA activate both Goa and Gob to inhibit cAMP accumulation, BnOCPA is selectively biased to the activation of Gob, with no discernible activation of Goa. Further quantification (Figure 2D, E, F) of this bias through the application of the operational model of receptor agonism (Black and Leff, 1983) to remove potential issues of system bias, confirmed selective activation of Gob by BnOCPA, with no detectable response at Goa (Figure 2F).

To establish the functional implications of BnOCPA's profound bias for Gob over Goa, we hypothesised that BnOCPA should reduce the actions of adenosine on the inhibition of cAMP accumulation via Goa. This was indeed the case (Figure 2G): BnOCPA antagonised the Goa-mediated inhibition of cAMP production by adenosine in a manner quantitatively similar (pK_i ~6.9) to its ability to bind to the hA_1R (pK_i ~6.6; Figure 1B). This observation, of the ability of BnOCPA to antagonise the actions of adenosine on cAMP inhibition, had parallels with the antagonising effects of BnOCPA on membrane potential in the CNS (Figure 1H, I; Figure S2A, C), and suggested that BnOCPA has the unique ability of displaying both agonist and antagonist-like properties.

The data from whole-cell patch-clamp recordings showed that BnOCPA did not influence neuronal membrane potential (Figure 1H, I), while experiments in recombinant hA_1Rs showed that BnOCPA did not activate Goa (Figure 2A, C-F). We thus predicted that A_1Rs in the hippocampus, where Gαo

is highly expressed (Jiang and Bajpayee, 2009; Terashima et al., 1988; Worley et al., 1986), particularly at extra-synaptic sites (Gabrion et al., 1989), should act via Goa to induce membrane hyperpolarisation. To test this we injected a series of previously validated interfering peptides (Gilchrist et al., 2002) against Goa and Gob into CA1 pyramidal cells during whole-cell voltage clamp recordings. Introduction of the Goa interfering peptide caused a significant attenuation of the adenosine-induced outward current (Figure 2H, J), whereas neither the scrambled peptide nor the Gob peptide had any effect on outward current amplitude (Figure 2I, J). Thus, membrane potential hyperpolarisation occurs mainly through A_1R activation of Goa. The data from recombinant receptors demonstrating the inability of BnOCPA to activate Goa (Figure 2A, C-F) thus explains why BnOCPA did not cause membrane hyperpolarisation, and indeed prevented or reversed the hyperpolarisation induced by CPA or adenosine, respectively (Figure 1H, I; Figure S2A, C).

The signalling bias displayed by BnOCPA is reflected in non-canonical binding modes and a selective interaction with Gαi/o subunits

To understand better the unusual signalling properties of BnOCPA and the highly specific Gα coupling, we carried out dynamic docking simulations to study the basic orthosteric binding mode of BnOCPA in an explicit, fully flexible environment using the active cryo-EM structure of the A_1R (PDB code 6D9H; Movie S1). We compared BnOCPA to the unbiased agonists adenosine and HOCPA, and an antagonist (PSB36) of the A_1R (Figure 3A-C). BnOCPA engaged the receptor with the same fingerprint as adenosine (Cheng et al., 2017) (Figure 3A) and HOCPA, (Figure 3B, Movie S2). Further explorations of the BnOCPA docked state using metadynamics (MD) simulations revealed interchangeable variations on this fingerprint (namely Modes A, B, and C; Figure 3D - F; Figure S6) that could be distinguished by the orientation of the BnOCPA-unique benzyl group. Having established the possible BnOCPA binding modes, we examined the respective contribution of the orthosteric agonists, the G protein α subunit α5 (C-terminal) helix (GαCT), and the Gα protein subunit (Flock et al., 2017; Okashah et al., 2019) to the empirically-observed G protein selectivity displayed by BnOCPA (Table 1, Figure 2C-H, Figure S3).

Simulations in the absence of G protein. Firstly, following Dror et al., (Dror et al., 2011) we compared the dynamics of the BnOCPA-bound A_1R with the corresponding dynamics of the receptor (Draper-Joyce et al., 2018; Glukhova et al., 2017) bound to either HOCPA (Figure 3B), the A_1R antagonist PSB36 (Figure 3C), or the apo receptor, our hypothesis being that there may be ligand-dependent differences in the way that the intracellular region of the receptor responds in the absence of the G protein. In these simulations the G protein was omitted so that inactivation was possible and so that the results were not G protein-dependent. The BnOCPA binding Modes A-C were interchangeable during MD simulations (Methods Table 1) but were associated with distinctly different dynamics, as monitored by changes in a structural hallmark of GPCR activation, the $N^{7.49}PXXY^{7.53}$ motif (Rosenbaum et al., 2009) (Figure S7). Given the high flexibility shown by the BnOCPA benzyl group during the simulations and its lipophilic character, we hypothesized and simulated a further binding mode (namely Mode D) not explored during MD simulations. This conformation involves a hydrophobic pocket underneath ECL3 (Figure 3G) which is responsible for the A_1/A_{2A} selectivity (Cheng et al., 2017). Superimposition of the four BnOCPA binding Modes A-D reveals the highly motile nature of the benzyl group of BnOCPA (Figure 3H) under the simulated conditions.

Quantification of the $N^{7.49}PXXY^{7.53}$ dynamics revealed that HOCPA, BnOCPA Mode A, BnOCPA Mode C and the apo receptor show a similar distribution of the RMSD of the conserved $N^{7.49}PXXY^{7.53}$ motif (Figure 3I; Figure S7). In contrast, the non-canonical BnOCPA binding Modes B and D were responsible for a partial transition of the $N^{7.49}PXXY^{7.53}$ backbone from the active conformation to the inactive conformation (Figure S7) in a manner analogous with the antagonist PSB36 (Figure 3J). Overall, the simulations revealed Mode D as the most stable BnOCPA pose (6.8 μs out 9 μs simulated starting from this configuration – Methods Table 1), while Mode B accounted for 3.6 μs out of 21 μs.

Dynamic Docking of GαCT. To simulate the agonist-driven interaction between the A_1R and the G protein, the α5 (C-terminal) helix (GαCT) of the G protein (Gi2, Goa, Gob) was dynamically docked to the HOCPA- and BnOCPA-bound active A_1R structure (again lacking G protein; Movie S3). This allowed us to evaluate the effect of different GαCT on the formation of the complex with A_1R to test

the hypothesis that, of Goa, Gob and Gi2, only the GαCT of Gob would fully engage with the BnOCPA-bound active A_1R, in line with the empirical observations of G protein selectivity summarized in Table 1. Figure 4A shows that the GαCT of Gob docked to the A_1R via a metastable state (MS1) relative to the canonical state (CS1; Movie S3), regardless of whether HOCPA or BnOCPA was bound. Figure 4B, C show that the CS1 geometry corresponds to the canonical arrangement as found in the cryo-EM A_1R:Gi protein complex, whereas state MS1 resembles the recently reported non-canonical state observed in the neurotensin receptor, believed to be an intermediate on the way to the canonical state (Kato et al., 2019). In contrast, Figure 4D-F show that the GαCT of Goa and Gi2 docks to the A_1R to form metastable states MS2 and MS3. MS2 is similar to the β_2-adrenergic receptor:GsCT fusion complex (Liu et al., 2019), proposed to be an intermediate on the activation pathway and a structure relevant to G protein specificity. In this case however, it appears to be on an unproductive pathway.

MD simulations on the full G protein Gα subunit. To test the hypothesis that the non-functional BnOCPA:A_1R:Goa complex showed anomalous dynamics, we increased the complexity of the simulations by considering the Gα subunit of the Goa and Gob protein bound to the A_1R:BnOCPA (Mode B or D) complex or the Gob protein bound to A_1R:HOCPA (a functional system). The most visible differences between Goa (Movie S4) and Gob (Movie S5) comprised the formation of transient hydrogen bonds between the α4-β6 and α3-β5 loops of Goa and helix 8 (H8) of the receptor (Table S3). Similar contacts are present in the non-canonical state of the neurotensin receptor:Gi protein complex (Kato et al., 2019). Overall, Goa interacted more with TM3 and ICL2 residues (Figure 4G, H), while TM5 and TM6, along with ICL1, were more engaged by Gob (Figure 4G, H). Interestingly, R291$^{7.56}$ and I292$^{8.47}$, which are located under the N$^{7.49}$PXXY$^{7.53}$ motif, showed a different propensity to interact with Goa or Gob. In this scenario, it is plausible that a particular A_1R conformation stabilized by BnOCPA (as suggested by the simulations in the absence of G protein, Figure 3I-J) may favor different intermediate states during the activation process of Goa and Gob.

In vivo physiological validation of BnOCPA-mediated signalling bias

Given BnOCPA's clear differential effects in a native physiological system (Figure 1), strong Gα bias (Figure 2), unique binding characteristics (Figure 3) and selective Gα interaction (Figure 4), we hypothesised that these properties might circumvent a key obstacle to the development of A_1R agonists for therapeutic use - their powerful effects in the cardiovascular system (CVS) where their activation markedly reduces both heart rate and blood pressure (Koeppen et al., 2009). As these cardiovascular effects are likely through Goa, which is expressed at high levels in the heart (Asano et al., 1995; Wolf et al., 1998) and plays an important role in regulating cardiac function (Jiang and Bajpayee, 2009), the lack of effect of BnOCPA on Goa (Figure 2A-F) predicted that BnOCPA would have minimal effects on the CVS. Moreover, given the antagonism of Goa-mediated actions by BnOCPA at native and recombinant A_1Rs (Figure 1H, I, Figure S2A, C, Figure 2G-J), we further predicted that the actions of adenosine on the CVS may be attenuated by BnOCPA.

In initial experiments we screened BnOCPA for its effects on heart rate using an isolated frog heart preparation. In contrast to adenosine and CPA, which depress heart rate through hyperpolarisation caused by activation of cardiac sinoatrial K^+ channels (Belardinelli et al., 1995), BnOCPA had no effect on heart rate, but markedly reduced the bradycardia evoked by adenosine (Figure S8A). Thus, BnOCPA appears not to activate A_1Rs in the heart, but instead behaves like an antagonist in preventing the actions of the endogenous agonist. These observations have parallels with BnOCPA's inability to activate A_1Rs to hyperpolarise neurones, and indeed inhibiting or reversing the postsynaptic hyperpolarisation induced by typical A_1R agonists (Figure 1G, H; Figure S2), and in preventing the A_1R/Goa-mediated inhibition of cAMP accumulation by adenosine (Figure 2I). Such antagonist-like behaviour may be explained by BnOCPA causing unique A_1R conformations unlike those of conventional agonists (Figure 3I, J), and driving non-canonical interactions with Goa (Figure 4).

To investigate the effects of BnOCPA in an intact mammalian system, we measured the influence of BnOCPA on heart rate and blood pressure in urethane-anaesthetised, spontaneously breathing adult rats. As expected, both resting heart rate and arterial blood pressure were significantly reduced by adenosine and CPA (Figure 5A to D). In complete contrast, BnOCPA had no effect on either heart rate (Figure 5A, C) or blood pressure (Figure 5B, D). Moreover, when co-applied with adenosine,

BnOCPA abolished the bradycardia induced by adenosine, indicating its ability to bind to the A_1R at the dose applied (Figure 5A, C; Figure S8B). The rapid early effects of adenosine on blood pressure, likely due to bradycardia, were blocked by BnOCPA, but the slower component was unaffected by BnOCPA (Figure 5B, D; Figure S8B). Volumes of saline equivalent to the drug injections had no effect on either heart rate or blood pressure and there was no waning in the effects of adenosine responses with repeated doses (Figure S8C, D). Thus, BnOCPA does not appear to act as an agonist at CVS A_1Rs, but instead antagonises the bradycardic effects of A_1R activation on the heart.

Since adverse effects on respiration (dyspnea) limit the use of systemic A_1R agonists (Sawynok, 2016), we additionally examined the effects of BnOCPA on respiration. In urethane-anaesthetised, spontaneously breathing adult rats, intravenous injection of the selective A_1R agonist CPA caused significant respiratory depression (Figure 6A to D). In stark contrast, BnOCPA had no appreciable effect on respiration (Figure 6A to D).

BnOCPA is a potent analgesic

Our observations of a lack of effect of BnOCPA on the CVS and respiration prompted an investigation into a potential application of A_1R agonists that had previously been severely curtailed by adverse cardiorespiratory events (Deb et al., 2019; Sawynok, 2016), namely the use of A_1R agonists as analgesics. Since sedation or motor impairment can be mistaken for analgesia, we tested BnOCPA in a sensitive assay for balance and motor coordination, the rotarod, in which the ability of a rodent to remain upon a slowly accelerating rotating cylinder is a measure of alertness and motor function. The ability of animals treated with morphine to remain on the rotating cylinder was strongly impaired (Figure 6E). In contrast, the performance of animals treated with BnOCPA, delivered either intravenously or intraperitoneally, was indistinguishable from vehicle-treated mice (Figure 6E). Thus, BnOCPA does not induce sedation or locomotor impairment that could confound interpretations of analgesia.

To assess the potential of BnOCPA as an analgesic, we used a rat model of chronic neuropathic pain (spinal nerve ligation) (Kim and Chung, 1992) a feature of which is mechanical allodynia

whereby the affected limb is rendered sensitive to previously innocuous tactile stimuli. Both intravenous (Figure 6F) and intrathecal (Figure 6G) BnOCPA potently reversed mechanical allodynia in a dose-dependent manner. Thus, BnOCPA exhibits powerful analgesic properties at doses devoid of sedative or cardiorespiratory effects, and at several orders of magnitude lower than the non-opioid analgesics pregabalin and gabapentin (Chincholkar, 2018).

Discussion

Biased agonists at GPCRs offer great potential for the selective activation of desirable intracellular signalling pathways, while avoiding, or indeed blocking those pathways that lead to adverse or unwanted effects (Kenakin, 2018). While this, and the potential to exploit previously unattractive drug targets such as the A_1R, have been appreciated, translation of *in vitro* observations, particularly of Gα bias, to native receptors *in vivo* has been problematic (Kenakin, 2018; Michel and Charlton, 2018). Here we have shown that translation of *in vitro* Gα signalling bias to an intact physiological system is possible. Moreover, this has occurred in the context of the A_1R, an attractive, but notoriously intractable drug target by virtue of the profound cardiorespiratory consequences of its activation.

Having identified BnOCPA as a biased agonist at recombinant A_1Rs *in vitro*, we established that this bias can be translated into the selective activation of native A_1Rs in both the *in vitro* CNS and *in vivo* cardiorespiratory and peripheral nervous systems. Moreover, these properties of BnOCPA were observed at A_1Rs expressed by three different species: amphibian, rat, and human. While BnOCPA bound to and induced A_1R coupling to Gαi/o subunits recruited by prototypical A_1R agonists such as adenosine and CPA, BnOCPA selectively activated Gob among the six Gαi/o subunits. This likely reflects BnOCPA's non-canonical binding profile at the A_1R, which had profound implications for the interaction with the GαCT in terms of different binding pathways and intermediate states, and in the different intra- and intermolecular hydrogen bond patterns and contacts observed in the simulations of the A_1R in complex with either Goa or Gob. These differences are likely to underlie the ability of the BnOCPA-bound A_1R to selectively trigger Gob activation among the six Gαi/o subtypes.

The unique and unprecedented G protein bias displayed by BnOPCA has physiological importance since it is able to inhibit excitatory synaptic transmission without causing neuronal membrane hyperpolarisation, sedation, bradycardia, hypotension or dyspnea. BnOCPA thus overcomes cardiovascular and respiratory obstacles to the development of adenosine-based therapeutics that have plagued the field since their first description nine decades ago (Drury and Szent-Gyorgyi, 1929). As a first, but significant, step towards this, we demonstrate that BnOCPA has powerful

analgesic properties in an *in vivo* model of chronic neuropathic pain, a condition for which the current treatments are either severely lacking in efficacy (Finnerup et al., 2018) or, in the case of opioids, come with unacceptable harms associated with adverse gastrointestinal effects, respiratory depression, tolerance, dependence and abuse potential (Imam et al., 2018).

We have thus shown that highly selective G protein biased agonism *in vitro* can be translated into selective activation of native A_1Rs to mediate differential physiological effects, and have identified a novel molecule capable of doing so. We have also explored molecular mechanisms by which this could occur, and demonstrated pain as one potential and wide-reaching therapeutic application. Such discoveries are of importance in both understanding GPCR-mediated signalling, and in the generation of both new research tools and therapeutics based on the untapped potential of biased agonists.

Acknowledgements: We gratefully acknowledge the support of the University of Warwick (URSS Awards to SH and JO; Warwick Ventures Proof of Concept Fund awards to MJW & BGF), the Leverhulme Trust (RPG-2017-255, CAR and GL to fund KB and GD), the BBSRC (BB/M00015X/2, GL and BB/M01116X/1, PhD studentship to EH), the MRC (MR/J003964/1; IW) and The Swiss National Science Foundation (PP00P2_146321, MLo). RH is supported by an MRC Discovery Award (MC_PC_15070). CAR is a Royal Society Industry Fellow. We would like to thank Stephen Hill, Stephen Briddon and Mark Soave (University of Nottingham) for gifting the Nluc-tagged adenosine receptor cell lines, the fluorescent antagonist AV039 and technical advice, and Kathleen Caron and Duncan Mackie (University of North Carolina) for the β-arrestin2-YFP construct. We are grateful to Professor Kevin Moffat and the Biochemistry students of the School of Life Sciences at the University of Warwick for access to their frog heart preparations, and to Professor Nick Dale, Dr Mark Wigglesworth, Dr Jens Kleinjung for discussions and comments on draft manuscripts, and Prof Arthur Christopoulos for a pre-publication copy of the adenosine A_1 cryo-EM structure. *In vivo* studies on neuropathic pain were funded and undertaken by NeuroSolutions Ltd.

Author Contributions: Experiments were designed by MJW, RH, CAR, GL, FYZ, DS, BGF, and were performed by MJW, EH, RH, KB, IW, HFW, WI, ED, CH, JO, SH. Compounds were synthesised by MLe, BP, MLo. Molecular docking simulations were carried out by GD and CAR. Work was originally conceived by MJW and BGF. The manuscript was written by MJW and BGF with comments on drafts from EH, RH, MLo, GL, IW, KB, GD, CAR, IM and DS.

Conflict of Interest: The University of Warwick has filed a patent application for uses of BnOCPA. FYZ, HFW and DS are employees and/or hold shares in NeuroSolutions.

Data Availability: The data and materials that support the findings of this study are available from the corresponding author upon reasonable request.

Supplementary Information:

Materials and Methods

Supplementary Figures S1 – S8

Supplementary Tables S1 – S3

Supplementary Movies S1 – S5

References

Asano, T., Shinohara, H., Morishita, R., Norota, I., Kato, K., and Endoh, M. (1995). The G-protein G(o) in mammalian cardiac muscle: localization and coupling to A1 adenosine receptors. J Biochem *117*, 183-189.

Aurelio, L., Baltos, J.A., Ford, L., Nguyen, A.T.N., Jorg, M., Devine, S.M., Valant, C., White, P.J., Christopoulos, A., May, L.T.*, et al.* (2018). A Structure-Activity Relationship Study of Bitopic N(6)-Substituted Adenosine Derivatives as Biased Adenosine A1 Receptor Agonists. J Med Chem *61*, 2087-2103.

Avet, C., Mancini, A., Breton, B., Le Gouill, C., Hauser, A.S., Normand, C., Kobayashi, H., Gross, F., Hogue, M., Lukasheva, V.*, et al.* (2020). Selectivity Landscape of 100 Therapeutically Relevant GPCR Profiled by an Effector Translocation-Based BRET Platform. bioRxiv, 2020.2004.2020.052027.

Baker, J.G., and Hill, S.J. (2007). A comparison of the antagonist affinities for the Gi- and Gs-coupled states of the human adenosine A1-receptor. J Pharmacol Exp Ther *320*, 218-228.

Baltos, J.A., Gregory, K.J., White, P.J., Sexton, P.M., Christopoulos, A., and May, L.T. (2016). Quantification of adenosine A(1) receptor biased agonism: Implications for drug discovery. Biochem Pharmacol *99*, 101-112.

Belardinelli, L., Shryock, J.C., Song, Y., Wang, D., and Srinivas, M. (1995). Ionic basis of the electrophysiological actions of adenosine on cardiomyocytes. FASEB J *9*, 359-365.

Black, J.W., and Leff, P. (1983). Operational models of pharmacological agonism. Proc R Soc Lond B Biol Sci *220*, 141-162.

Borea, P.A., Gessi, S., Merighi, S., Vincenzi, F., and Varani, K. (2018). Pharmacology of Adenosine Receptors: The State of the Art. Physiol Rev *98*, 1591-1625.

Cheng, R.K.Y., Segala, E., Robertson, N., Deflorian, F., Doré, A.S., Errey, J.C., Fiez-Vandal, C., Marshall, F.H., and Cooke, R.M. (2017). Structures of Human A1 and A2A Adenosine Receptors with Xanthines Reveal Determinants of Selectivity. Structure *25*, 1275-1285.e1274.

Chincholkar, M. (2018). Analgesic mechanisms of gabapentinoids and effects in experimental pain models: a narrative review. Br J Anaesth *120*, 1315-1334.

Ciruela, F., Saura, C., Canela, E.I., Mallol, J., Lluis, C., and Franco, R. (1997). Ligand-induced phosphorylation, clustering, and desensitization of A1 adenosine receptors. Mol Pharmacol *52*, 788-797.

Congreve, M., de Graaf, C., Swain, N.A., and Tate, C.G. (2020). Impact of GPCR Structures on Drug Discovery. Cell *181*, 81-91.

Cordeaux, Y., Ijzerman, A.P., and Hill, S.J. (2004). Coupling of the human A1 adenosine receptor to different heterotrimeric G proteins: evidence for agonist-specific G protein activation. Br J Pharmacol *143*, 705-714.

Deb, P.K., Deka, S., Borah, P., Abed, S.N., and Klotz, K.N. (2019). Medicinal Chemistry and Therapeutic Potential of Agonists, Antagonists and Allosteric Modulators of A1 Adenosine Receptor: Current Status and Perspectives. Curr Pharm Des *25*, 2697-2715.

Draper-Joyce, C.J., Khoshouei, M., Thal, D.M., Liang, Y.L., Nguyen, A.T.N., Furness, S.G.B., Venugopal, H., Baltos, J.A., Plitzko, J.M., Danev, R.*, et al.* (2018). Structure of the adenosine-bound human adenosine A1 receptor-Gi complex. Nature *558*, 559-563.

Dror, R.O., Arlow, D.H., Maragakis, P., Mildorf, T.J., Pan, A.C., Xu, H., Borhani, D.W., and Shaw, D.E. (2011). Activation mechanism of the β2-adrenergic receptor. Proc Natl Acad Sci USA *108*, 18684-18689.

Drury, A.N., and Szent-Gyorgyi, A. (1929). The physiological activity of adenine compounds with especial reference to their action upon the mammalian heart. J Physiol *68*, 213-237.

Dunwiddie, T.V., and Masino, S.A. (2001). The role and regulation of adenosine in the central nervous system. Annu Rev Neurosci *24*, 31-55.

Escriche, M., Burgueno, J., Ciruela, F., Canela, E.I., Mallol, J., Enrich, C., Lluis, C., and Franco, R. (2003). Ligand-induced caveolae-mediated internalization of A1 adenosine receptors: morphological evidence of endosomal sorting and receptor recycling. Exp Cell Res *285*, 72-90.

Ferguson, G., Watterson, K.R., and Palmer, T.M. (2002). Subtype-specific regulation of receptor internalization and recycling by the carboxyl-terminal domains of the human A1 and rat A3 adenosine receptors: consequences for agonist-stimulated translocation of arrestin3. Biochemistry *41*, 14748-14761.

Finnerup, N.B., Haroutounian, S., Baron, R., Dworkin, R.H., Gilron, I., Haanpaa, M., Jensen, T.S., Kamerman, P.R., McNicol, E., Moore, A.*, et al.* (2018). Neuropathic pain clinical trials: factors associated with decreases in estimated drug efficacy. Pain *159*, 2339-2346.

Flock, T., Hauser, A.S., Lund, N., Gloriam, D.E., Balaji, S., and Babu, M.M. (2017). Selectivity determinants of GPCR-G-protein binding. Nature *545*, 317-322.

Gabrion, J., Brabet, P., Nguyen Than Dao, B., Homburger, V., Dumuis, A., Sebben, M., Rouot, B., and Bockaert, J. (1989). Ultrastructural localization of the GTP-binding protein Go in neurons. Cell Signal *1*, 107-123.

Gilchrist, A., Li, A., and Hamm, H.E. (2002). G alpha COOH-terminal minigene vectors dissect heterotrimeric G protein signaling. Sci STKE *2002*, pl1.

Gines, S., Ciruela, F., Burgueno, J., Casado, V., Canela, E.I., Mallol, J., Lluis, C., and Franco, R. (2001). Involvement of caveolin in ligand-induced recruitment and internalization of A(1) adenosine receptor and adenosine deaminase in an epithelial cell line. Mol Pharmacol *59*, 1314-1323.

Glukhova, A., Thal, D.M., Nguyen, A.T., Vecchio, E.A., Jorg, M., Scammells, P.J., May, L.T., Sexton, P.M., and Christopoulos, A. (2017). Structure of the Adenosine A1 Receptor Reveals the Basis for Subtype Selectivity. Cell *168*, 867-877 e813.

Hauser, A.S., Attwood, M.M., Rask-Andersen, M., Schiöth, H.B., and Gloriam, D.E. (2017). Trends in GPCR drug discovery: new agents, targets and indications. Nature Reviews Drug Discovery *16*, 829.

Headrick, J.P., Ashton, K.J., Rose'meyer, R.B., and Peart, J.N. (2013). Cardiovascular adenosine receptors: expression, actions and interactions. Pharmacol Ther *140*, 92-111.

Hill, S.J., and Baker, J.G. (2003). The ups and downs of Gs- to Gi-protein switching. Br J Pharmacol *138*, 1188-1189.

Iacovelli, L., Franchetti, R., Grisolia, D., and De Blasi, A. (1999). Selective regulation of G protein-coupled receptor-mediated signaling by G protein-coupled receptor kinase 2 in FRTL-5 cells: analysis of thyrotropin, alpha(1B)-adrenergic, and A(1) adenosine receptor-mediated responses. Mol Pharmacol *56*, 316-324.

Imam, M.Z., Kuo, A., Ghassabian, S., and Smith, M.T. (2018). Progress in understanding mechanisms of opioid-induced gastrointestinal adverse effects and respiratory depression. Neuropharmacology *131*, 238-255.

Jacobson, K.A., and Muller, C.E. (2016). Medicinal chemistry of adenosine, P2Y and P2X receptors. Neuropharmacology *104*, 31-49.

Jiang, M., and Bajpayee, N.S. (2009). Molecular mechanisms of Go signaling. Neurosignals *17*, 23-41.

Kato, H.E., Zhang, Y., Hu, H., Suomivuori, C.M., Kadji, F.M.N., Aoki, J., Krishna Kumar, K., Fonseca, R., Hilger, D., Huang, W.*, et al.* (2019). Conformational transitions of a neurotensin receptor 1-Gi1 complex. Nature *572*, 80-85.

Kenakin, T. (2018). Is the Quest for Signaling Bias Worth the Effort? Mol Pharmacol *93*, 266-269.

Kenakin, T. (2019). Biased Receptor Signaling in Drug Discovery. Pharmacol Rev *71*, 267-315.

Kim, S.H., and Chung, J.M. (1992). An experimental model for peripheral neuropathy produced by segmental spinal nerve ligation in the rat. Pain *50*, 355-363.

Kliewer, A., Gillis, A., Hill, R., Schmiedel, F., Bailey, C., Kelly, E., Henderson, G., Christie, M.J., and Schulz, S. (2020). Morphine-induced respiratory depression is independent of beta-arrestin2 signalling. Br J Pharmacol *177*, 2923-2931.

Knight, A., Hemmings, J.L., Winfield, I., Leuenberger, M., Frattini, E., Frenguelli, B.G., Dowell, S.J., Lochner, M., and Ladds, G. (2016). Discovery of novel adenosine receptor agonists that exhibit subtype selectivity. J Med Chem *59*, 947-964.

Koeppen, M., Eckle, T., and Eltzschig, H.K. (2009). Selective deletion of the A1 adenosine receptor abolishes heart-rate slowing effects of intravascular adenosine in vivo. PLoS One *4*, e6784.

Liu, X., Xu, X., Hilger, D., Aschauer, P., Tiemann, J.K.S., Du, Y., Liu, H., Hirata, K., Sun, X., Guixa-Gonzalez, R.*, et al.* (2019). Structural Insights into the Process of GPCR-G Protein Complex Formation. Cell *177*, 1243-1251 e1212.

Michel, M.C., and Charlton, S.J. (2018). Biased Agonism in Drug Discovery-Is It Too Soon to Choose a Path? Mol Pharmacol *93*, 259-265.

Okashah, N., Wan, Q., Ghosh, S., Sandhu, M., Inoue, A., Vaidehi, N., and Lambert, N.A. (2019). Variable G protein determinants of GPCR coupling selectivity. Proc Natl Acad Sci U S A *116*, 12054-12059.

Rosenbaum, D.M., Rasmussen, S.G., and Kobilka, B.K. (2009). The structure and function of G-protein-coupled receptors. Nature *459*, 356-363.

Sawynok, J. (2016). Adenosine receptor targets for pain. Neuroscience *338*, 1-18.

Slosky, L.M., Bai, Y., Toth, K., Ray, C., Rochelle, L.K., Badea, A., Chandrasekhar, R., Pogorelov, V.M., Abraham, D.M., Atluri, N.*, et al.* (2020). beta-Arrestin-Biased Allosteric Modulator of NTSR1 Selectively Attenuates Addictive Behaviors. Cell.

Stewart, G.D., Valant, C., Dowell, S.J., Mijaljica, D., Devenish, R.J., Scammells, P.J., Sexton, P.M., and Christopoulos, A. (2009). Determination of adenosine A1 receptor agonist and antagonist pharmacology using Saccharomyces cerevisiae: implications for ligand screening and functional selectivity. J Pharmacol Exp Ther *331*, 277-286.

Terashima, T., Katada, T., Oinuma, M., Inoue, Y., and Ui, M. (1988). Immunohistochemical analysis of the localization of guanine nucleotide-binding protein in the mouse brain. Brain Res *442*, 305-311.

Valant, C., May, L.T., Aurelio, L., Chuo, C.H., White, P.J., Baltos, J.A., Sexton, P.M., Scammells, P.J., and Christopoulos, A. (2014). Separation of on-target efficacy from adverse effects through rational design of a bitopic adenosine receptor agonist. Proc Natl Acad Sci U S A *111*, 4614-4619.

Varani, K., Vincenzi, F., Merighi, S., Gessi, S., and Borea, P.A. (2017). Biochemical and Pharmacological Role of A1 Adenosine Receptors and Their Modulation as Novel Therapeutic Strategy. Adv Exp Med Biol *1051*, 193-232.

Vecchio, E.A., Baltos, J.A., Nguyen, A.T.N., Christopoulos, A., White, P.J., and May, L.T. (2018). New paradigms in adenosine receptor pharmacology: allostery, oligomerization and biased agonism. Br J Pharmacol *175*, 4036-4046.

Violin, J.D., and Lefkowitz, R.J. (2007). Beta-arrestin-biased ligands at seven-transmembrane receptors. Trends Pharmacol Sci *28*, 416-422.

Weltha, L., Reemmer, J., and Boison, D. (2018). The role of adenosine in epilepsy. Brain Res Bull.

Wise, A., Sheehan, M., Rees, S., Lee, M., and Milligan, G. (1999). Comparative analysis of the efficacy of A1 adenosine receptor activation of Gi/o alpha G proteins following coexpression of receptor and G protein and expression of A1 adenosine receptor-Gi/o alpha fusion proteins. Biochemistry *38*, 2272-2278.

Wolf, W.P., Spicher, K., Haase, H., and Schulze, W. (1998). Immunocytochemical localization of the G-protein sub-unit, G(o) alpha, in rat heart. Implications for a role of G(o) alpha in secretion of cardiac hormones. J Mol Cell Cardiol *30*, 1149-1162.

Wootten, D., Christopoulos, A., Marti-Solano, M., Babu, M.M., and Sexton, P.M. (2018). Mechanisms of signalling and biased agonism in G protein-coupled receptors. Nat Rev Mol Cell Biol *19*, 638-653.

Worley, P.F., Baraban, J.M., Van Dop, C., Neer, E.J., and Snyder, S.H. (1986). Go, a guanine nucleotide-binding protein: immunohistochemical localization in rat brain resembles distribution of second messenger systems. Proc Natl Acad Sci U S A *83*, 4561-4565.

Yin, W., Li, Z., Jin, M., Yin, Y.L., de Waal, P.W., Pal, K., Yin, Y., Gao, X., He, Y., Gao, J.*, et al.* (2019). A complex structure of arrestin-2 bound to a G protein-coupled receptor. Cell Res *29*, 971-983.

Table 1

Agonist	IC_{50} (nM)	Gα subunits					
		Gi1	Gi2	Gi3	Goa	Gob	Gz
Adenosine	3.5						
CPA	0.6						
NECA	0.8						
HOCPA	0.8						
BnOCPA	0.7						

Summary of Gα activation by selective A_1R agonists; Green boxes indicate activation; Grey boxes indicated no activation. Indicative IC_{50} values for inhibition of cAMP production in CHO-K1 cells derived from the mean pIC_{50} values reported in Table S1. Data taken from: Adenosine, CPA, BnOCPA Figure 1, Figure S3; NECA, Figure S3; HOCPA, Figure S4.

Figure 1. BnOCPA discriminates between pre- and postsynaptic A_1Rs in the CNS

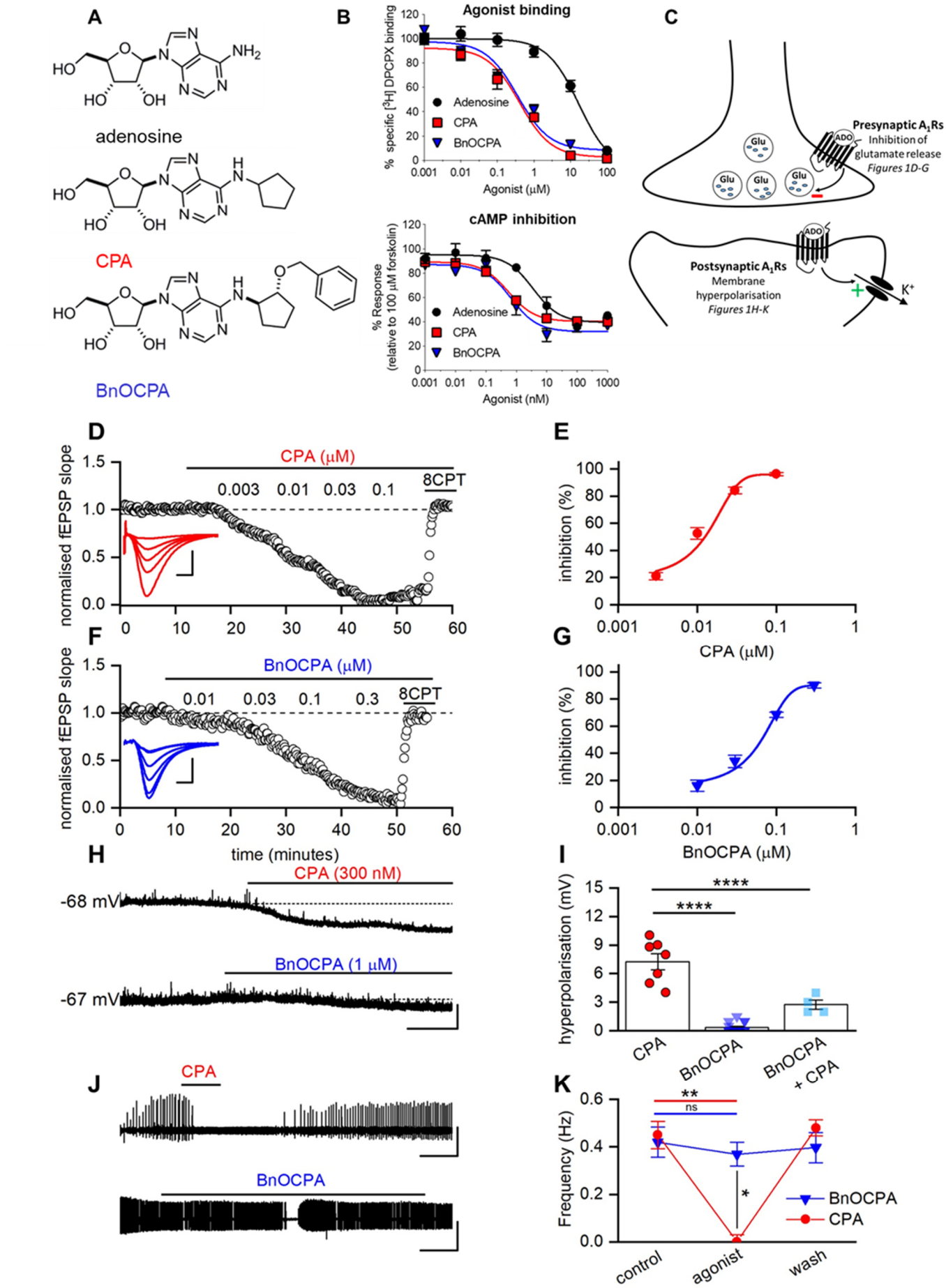

Figure 1. BnOCPA discriminates between pre- and postsynaptic A_1Rs in the CNS

(A) Chemical structures of adenosine, CPA and its derivative, BnOCPA (Knight et al., 2016). **(B; *Top panel)*** The binding of adenosine, CPA and BnOCPA to the human (h) A_1R was measured via their ability to displace [^{3}H]DPCPX, a selective antagonist for the A_1R, from membranes prepared from CHO-K1-hA_1R cells. The data indicate that CPA and BnOCPA bind with equal affinity to the A_1R (pK_i ~6.6), while adenosine has a reduced affinity (pK_i ~5; *n* = 5 - 19 individual repeats). **(B: *Lower panel*)** cAMP levels were measured in CHO-K1-hA_1R cells following co-stimulation with 1 µM forskolin and each compound (1 pM - 1 µM) for 30 minutes. This identified that all are full agonists at the hA_1R. Adenosine displayed a 10-fold reduced potency compared to CPA and BnOCPA (*n* = 4 individual repeats). **(C)** Diagram illustrating pre- and postsynaptic A_1Rs at hippocampal synapses, their physiological effects upon activation, and the panels in Figure 1 where these effects can be seen (presynaptic: panels **D - G**; postsynaptic: panels **H – K**). **(D)** Increasing concentrations of the A_1R agonist CPA reduced the field excitatory postsynaptic potential (fEPSP), an effect reversed by the A_1R antagonist 8CPT (2 µM). The graph plots the normalised negative slope of the fEPSP, an index of the strength of synaptic transmission, over time. Inset, superimposed fEPSP averages in control (largest fEPSP) and becoming smaller in increasing concentrations of CPA. Scale bars measure 0.2 mV and 5 ms. **(E)** Concentration-response curve for the inhibition of synaptic transmission by CPA (IC_{50} = 11.8 ± 2.7 nM; *n* = 11 slices). **(F)** Increasing concentrations of BnOCPA reduced the fEPSP, an effect reversed by 8CPT (2 µM). Inset, superimposed fEPSP averages in control and in increasing concentrations of BnOCPA. Scale bars measure 0.1 mV and 2 ms. **(G)** Concentration-response curve for the inhibition of synaptic transmission by BnOCPA (IC_{50} = 65 ± 0.3 nM; *n* = 11 slices). **(H)** CPA (300 nM) hyperpolarised the membrane potential while BnOCPA (1 µM) had little effect. Scale bars measure 4 mV and 30 s. **(I)** Summary data for membrane potential changes. The mean hyperpolarisation produced by CPA (300 nM; 7.26 ± 0.86 mV, *n* = 7 cells) was significantly different (one-way ANOVA; F(2,23) = 70.46; P = 1.55 x 10^{-10}) from that produced by BnOCPA (300 nM - 1 µM; 0.33 ± 0.14 mV, *n* = 10 and 5 cells, respectively; P = 8.26 x 10^{-11}) and for CPA (300 nM) applied in the presence of BnOCPA (300 nM; 2.75 ± 0.48 mV, n = 4 cells, P = 2.89 x 10^{-5}; Figure 2A for an example trace). **(J)** In an *in vitro* model of seizure activity, represented as

frequent spontaneous spiking from baseline, CPA (300 nM) reversibly blocked activity while BnOCPA (300 nM) had little effect. Scale bars measure 0.5 mV and 200 s. **(K)** Summary data for seizure activity expressed in terms of the frequency of spontaneous spiking before, during and after CPA or BnOCPA. CPA abolished seizure activity (n = 4) whereas BnOCPA did not significantly reduce seizure frequency (n = 6). Data represented as mean ± SEM; Two-way RM ANOVA (BnOCPA vs CPA slices): $F(1, 3) = 186.11$, $P = 8.52 \times 10^{-4}$ with the following Bonferroni post hoc comparisons: BnOCPA vs Control; P = 1; CPA vs control; P = 0.010; BnOCPA vs CPA; P = 0.027. Averaged data is presented as mean ± SEM. ns, not significant; ∗, P < 0.05; ∗∗, P < 0.02; ∗∗∗∗, P < 0.0001.

See also Figures S1 and S2, and Tables S1 and S2

Figure 2. BnOCPA selectively activates Gob.

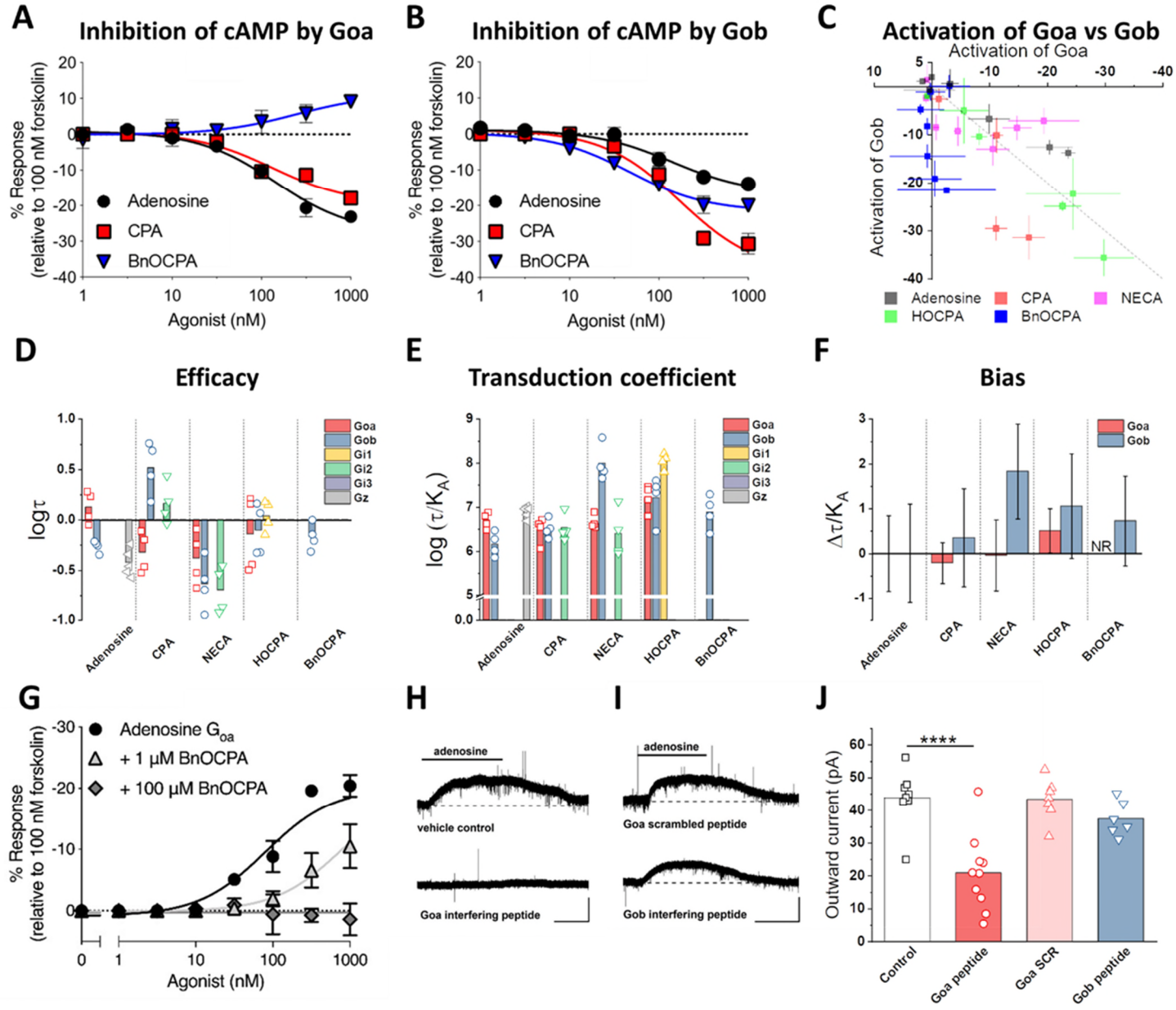

Figure 2. BnOCPA selectively activates Gob.

(A) cAMP accumulation was measured in PTX-pre-treated (200 ng/ml) CHO-K1-hA_1R cells expressing PTX-insensitive Goa following co-stimulation with 1 μM forskolin and each compound (1 pM - 1 μM) for 30 minutes (*n* = 6 individual repeats). The data demonstrates that BnOCPA does not activate Goa. **(B)**, as for **(A)**, but cells were transfected with PTX-insensitive Gob. Adenosine, CPA and BnOCPA all inhibit cAMP accumulation through coupling to Gob (*n* = 6 individual repeats). Stimulation of cAMP production in **A** reflects BnOCPA's activation of endogenous, PTX-resistant Gαs by the A_1R and is in agreement with previous observations for other A_1R agonists (see Figure S3 and (Baker and Hill, 2007; Cordeaux et al., 2004; Hill and Baker, 2003)). **(C)** The inhibition of cAMP accumulation via A_1R:Goa or A_1R:Gob by A_1R agonists is plotted at each concentration of agonist. No bias (equal activation of Goa and Gob at each concentration) would fall on the line of identity (broken grey line). HOCPA behaves most like an unbiased agonist, with some bias for Gob shown by CPA, and for Goa by adenosine. NECA displays concentration-dependent bias at both Goa and Gob. BnOCPA is highly biased towards Gob, with no activation of Goa. Data presented as mean ± SEM and is replotted from Figures S3 and S4. **(D)** Bar chart showing the efficacy of each agonist at individual A_1R-Gαi/o complexes as determined using the operational model of agonism (Black and Leff, 1983). BnOCPA is only efficacious via Gob-coupled A_1Rs. **(E)** Bar chart showing the transduction coefficient (log (τ/K_A)) for each agonist at individual A_1R-Gαi/o complexes. Signal transduction by BnOCPA only occurs via Gob. **(F)** Signalling bias for A_1R-Goa and A_1R-Gob was determined relative to the natural agonist adenosine using the change in log (τ/K_A) ratio for the data in **E**. Compared to adenosine, and unlike NECA, BnOCPA elicits no measurable response (NR) at Goa. **(G)** Adenosine's ability to inhibit cAMP accumulation via its activation of Goa was inhibited by BnOCPA in a concentration-dependent manner and with a K_d of 113 nM (pK_i ~6.9 (*n* = 4 individual repeats) similar to the binding affinity to the hA_1R pK_i ~6.6; Figure 1B). **(H)** Example current traces produced by adenosine (10 μM) in control conditions or in the presence of intracellular Goa interfering peptide (100 μM) Scale bar measures 50 pA and 100 s. **(I)** Example current traces produced by adenosine (10 μM) in the presence of scrambled Goa peptide (100 μM) or Gob interfering peptide (100 μM). Scale bar measure 50 pA and 100 s. **(J)** Summary data of adenosine-

induced outward current experiments. The mean amplitude of the outward current induced by adenosine (43.9 ± 3.1 pA, *n* = 8 cells) was significantly reduced (one-way ANOVA; F(3,27) = 13.31, P = 1.60x 10^{-5}) to 20.9 ± 3.6 pA (*n* = 10 cells, P = 5.35 x 10^{-5}) in 100 μM Goa interfering peptide. Neither the scrambled Goa peptide (Goa-SCR; 43.4 ± 2.4 pA, *n* = 7 cells, P = 1) nor the Gob interfering peptide (37. 4 ± 2.2 pA, *n* = 6 cells, P = 1) significantly reduced the amplitude of the adenosine-induced outward current. Averaged data is presented as mean ± SEM. ****, P < 0.0001. See also Figures S3, S4 and S5

Figure 3. Molecular dynamics simulations reveal that BnOCPA binding modes can uniquely drive both agonist- and antagonist-like intracellular conformations of the A_1R.

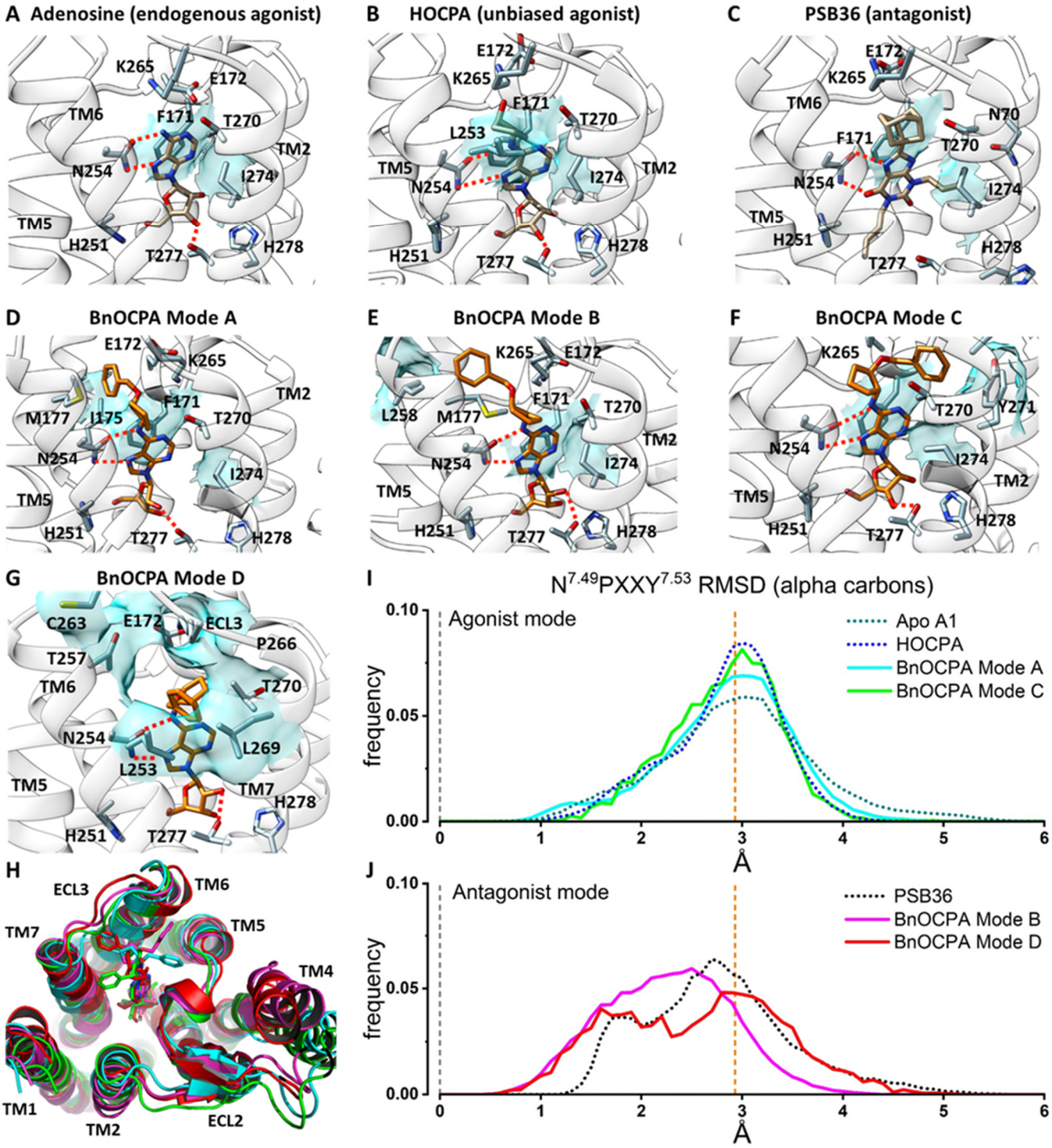

Figure 3. Molecular dynamics simulations reveal that BnOCPA binding modes can uniquely drive both agonist- and antagonist-like intracellular conformations of the A_1R.

(A) Adenosine binding pose: $N254^{6.55}$ (Ballesteros-Weinstein superscript enumeration) is engaged in key hydrogen bonds, while important hydrophobic contacts are shown as cyan transparent surfaces ($F171^{ECL2}$ and $I274^{7.39}$). **(B)** On the basis of structural similarities and the dynamic docking (Movie S2), HOCPA was predicted to bind with a geometry analogous to adenosine; the cyclopentyl group makes further hydrophobic contacts with $L253^{6.54}$, as shown by simulation. **(C)** The xanthine scaffold of the antagonist PSB36 makes hydrogen bonds with $N254^{6.55}$ side chains and hydrophobic contacts with $F171^{ECL2}$ and $I274^{7.39}$. **(D)** BnOCPA agonist-like binding Mode A (Movie S1): the benzyl group orients towards the ECL2 and makes hydrophobic contacts with $I175^{ECL2}$ (and $M177^{5.35}$) side chains. **(E)** BnOCPA antagonist-like binding Mode B: the benzyl group orients towards the top of TM5/TM6 and makes hydrophobic contacts with $L258^{6.59}$ side chain. **(F)** BnOCPA agonist-like binding Mode C: the benzyl group orients towards the top of TM7 and makes hydrophobic contacts with $Y271^{7.36}$ side chain. **(G)** Binding orientation of BnOCPA in antagonist Mode D: the benzyl group orients under ECL3 and occupies the hydrophobic pocket defined by $L253^{6.54}$, $T257^{6.58}$, $T270^{7.35}$, and $L269^{7.34}$. Key hydrogen bonds with $N254^{6.55}$ and $T277^{7.42}$ are shown as dotted lines; main hydrophobic contacts are highlighted as cyan transparent surfaces. **(H)** Extracellular view of the A_1R showing the four BnOCPA binding Modes A (cyan), B (magenta), C (green), and D (red) as randomly extracted from the MD simulations. **(I, J)** Root-mean-square deviation (RMSD) distributions considering the inactive $N^{7.49}PXXY^{7.53}$ motif on the distal part of TM7 as reference. **(I)** HOCPA (blue broken line), BnOCPA Mode A (cyan curve), BnOCPA Mode C (green curve) and the apo receptor (dark green broken line) have a common distribution centring around the active confirmation of the A_1R (orange broken line; Figure S7). In contrast, **(J)** PSB36 (black broken line), BnOCPA Mode B (magenta curve) and BnOCPA Mode D (red curve) RMSD values have the tendency to move closer to the inactive $N^{7.49}PXXY^{7.53}$ geometry (leftward shift of the curves towards broken grey line at x = 0).

See also Figures S6 and S7, Movies S1 and S2 and Methods Table 1.

Figure 4. BnOCPA selectively induces canonical activation states at A_1R:Gob, but non-productive metastable states at other Gαi/o subunits.

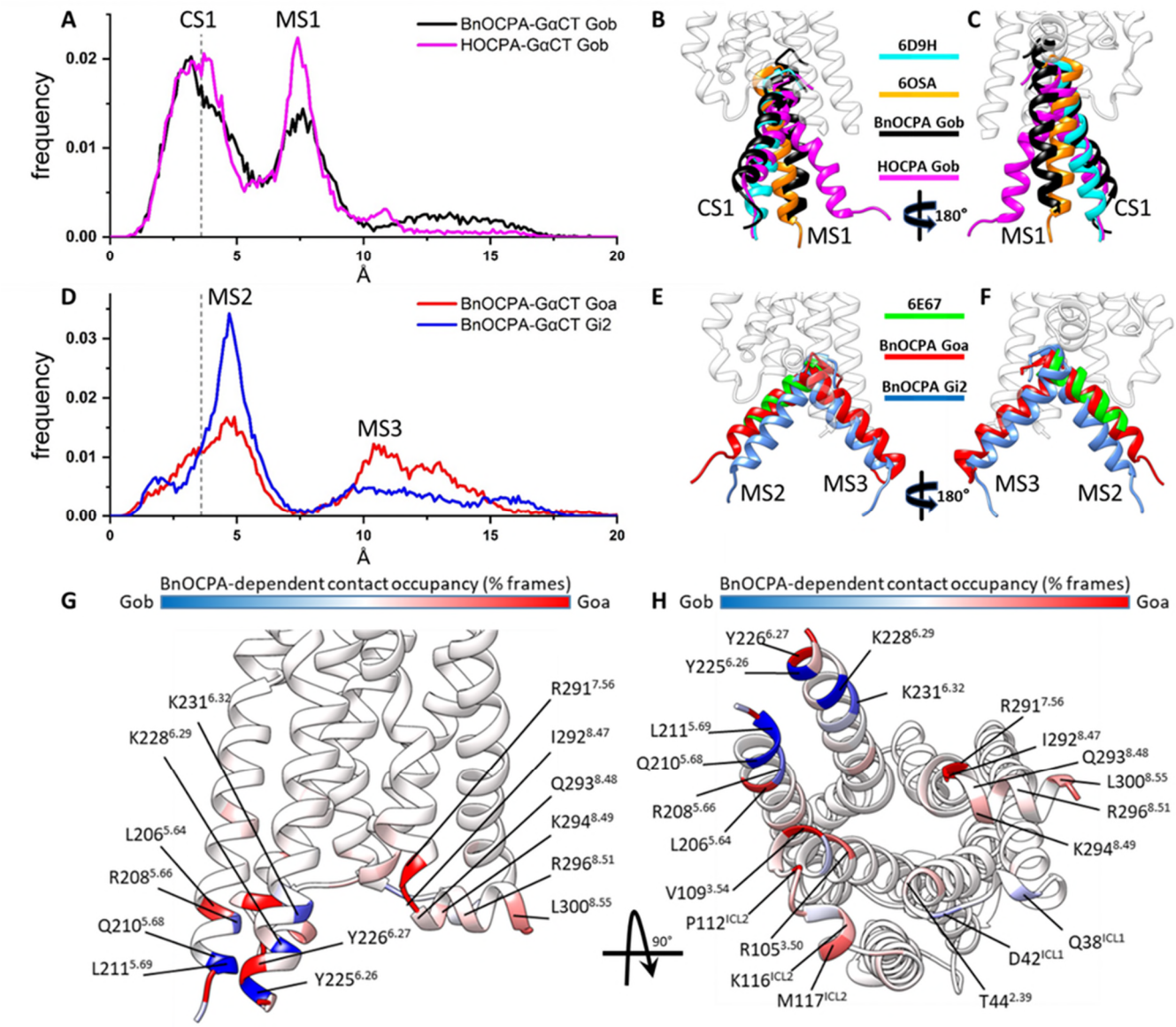

Figure 4. BnOCPA selectively induces canonical activation states at A_1R:Gob, but non-productive metastable states at other Gαi/o subunits.

(A, B, C) Dynamic docking of the Gob GαCT (last 27 residues) performed on the BnOCPA-A_1R (black) and the HOCPA-A_1R (magenta) complex, respectively. **(A)** Frequency distribution of the RMSD of the last 15 residues of GαCT (alpha carbon atoms) to the Gi2 GαCT conformation reported in the A_1R cryo-EM structure 6D9H (the 3.6Å resolution of which is indicated by the dashed grey line): the two most probable RMSD ranges, namely canonical state CS1 and metastable state MS1, can be observed. **(B, C)** Two side views of representative MD frames of the most populated α5 clusters from the states CS1 and MS1. The last 15 residues of Gob GαCT in the CS1 states of both BnOCPA (black) and HOCPA (magenta) resemble the experimental Gi2 bound state (PDB code 6D9H - cyan). The alternative highly populated MS1 state is characterized by a binding geometry similar to the non canonical Gi intermediate state reported in the neurotensin receptor structure 6OSA (orange). **(D, E, F)** Dynamic docking of the Goa (red) and Gi2 (blue) GαCT (last 27 residues) performed on the BnOCPA-A_1R complex. **(D)** Frequency distribution of the RMSD of the GαCT last 15 residues (alpha carbon atoms) to the Gi2 GαCT conformation reported in the A_1R cryo-EM structure 6D9H (the resolution of which, 3.6Å, is indicated by the dashed grey line): the two most probable RMSD ranges are labelled as MS2 and MS3. **(E, F)** Two side views of representative MD frames of the most populated GαCT clusters from the states MS2 and MS3; the Goa (red) and Gi2 (blue) last 15 residues in the state MS2 overlap well with the putative Gs intermediate state (PDB code 6E67 - green). In the alternative highly populated state MS3, the GαCT helix orients in unique conformations that differ from those previously described. **(G, H)** For each residue the interaction plotted on the backbone is the difference between the Goa and Gob occupancies in the presence of orthosteric BnOCPA (% of MD frames in which interaction occurred). BnOCPA/A_1R/Goa had the tendency to more interact with ICL2, TM3 TM7, and H8 (red), while BnOCPA/A_1R/Gob formed more contacts with TM5 and TM6 (blue).

See also Table S3, and Movies S3, S4 and S5.

Figure 5. BnOCPA does not affect heart rate or blood pressure

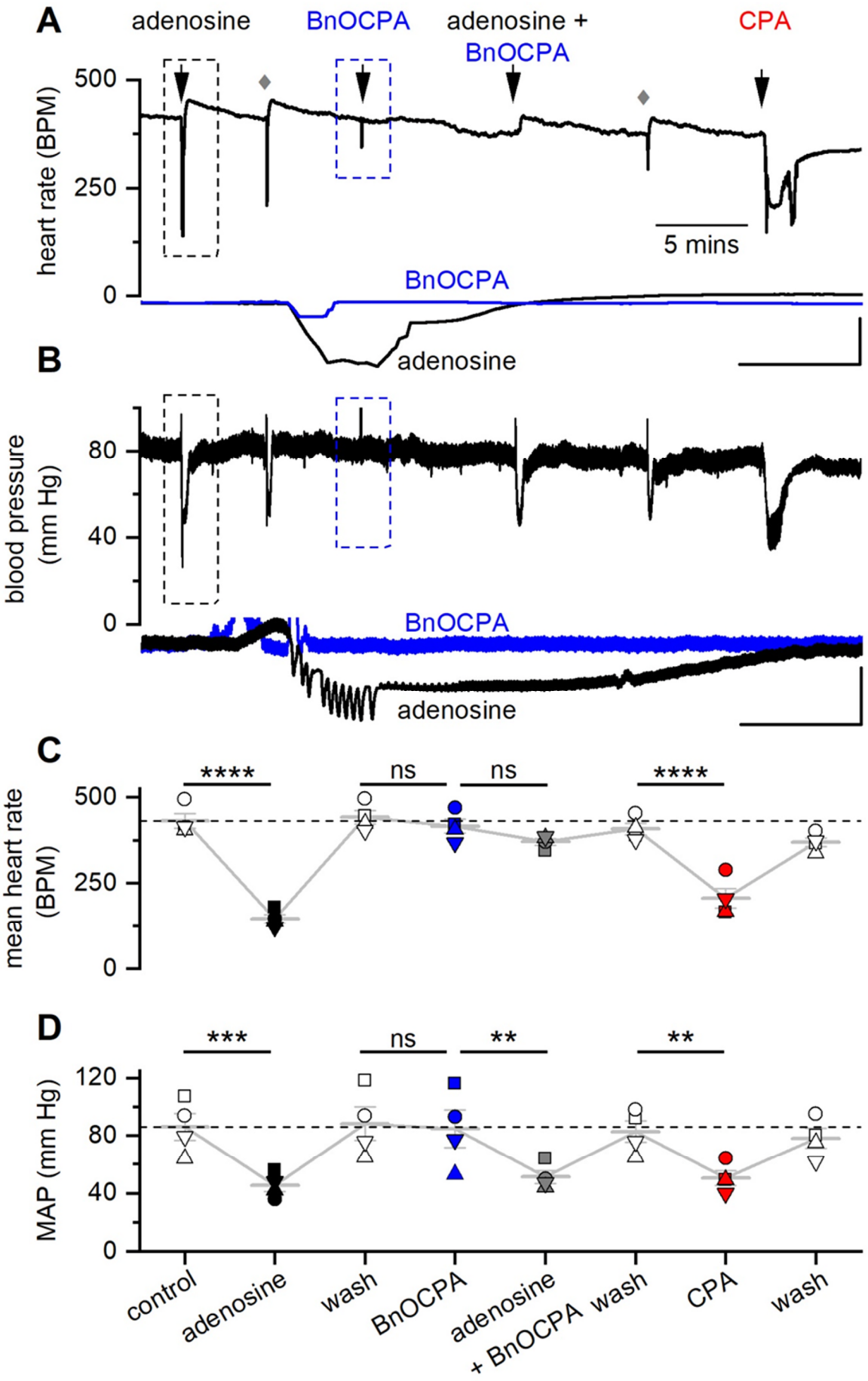

Figure 5. BnOCPA does not affect heart rate or blood pressure

(A) Examples of heart rate (HR) and **(B)** blood pressure traces from a single urethane-anaesthetised, spontaneously breathing rat showing the effects of adenosine (1 mg·kg^{-1}), BnOCPA (8.3 µg·kg^{-1}) and CPA (6.3 µg·kg^{-1}). Adenosine, BnOCPA and CPA were all given as a 350 µL·kg^{-1} IV bolus. The intravenous cannula was flushed with 0.9% saline (grey diamonds) to remove compounds in the tubing. The overshoot in HR following adenosine applications is likely the result of the baroreflex. Insets are expanded HR and blood pressure responses to adenosine (black trace, boxed region in **A** and **B**) and BnOCPA (blue trace and boxed region in **A** and **B**). Scale bars measure: HR, 200 BPM and 6 s; blood pressure, 40 mm Hg and 6 s. **(C, D)** Summary data for 4 experiments. Data from each rat is shown as a different symbol. Means (± SEM, light grey bars) are connected to indicate the sequential nature of treatments across the four preparations. One-way RM ANOVA for: **(C)** HR, Greenhouse-Geisser corrected $F(2.33, 7.00) = 68.27$, $P = 2.07 \times 10^{-5}$; **(D)** mean arterial blood pressure (MAP), Greenhouse-Geisser corrected $F(1.84, 5.52) = 10.51$, $P = 0.014$; with the following Bonferroni post hoc comparisons: The resting HR of 432 ± 21 BPM was significantly reduced to 147 ± 12 BPM (~66 %, $P = 2.76 \times 10^{-11}$) by adenosine. BnOCPA had no significant effect on HR (~6%, 442 ± 20 vs 416 ± 21 BPM; P = 1) but prevented the bradycardic effects of adenosine ($P = 2.71 \times 10^{-9}$ vs adenosine) when co-injected (mean change 51 ± 4 BPM; ~12 %; P = 0.67). CPA significantly decreased HR (from 408 ± 17 to 207 ± 29 BPM; ~50 %, $P = 1.85 \times 10^{-8}$), a decrease that was not significantly different to the effect of adenosine (P = 0.12), but was significantly different to the effect of both BnOCPA ($P = 9.00 \times 10^{-9}$) and adenosine in the presence of BnOCPA ($P = 6.69 \times 10^{-7}$). The resting MAP (86 ± 9 mm Hg) was significantly reduced by adenosine (~47 %, 46 ± 4 mm Hg; P = 0.001). BnOCPA had no significant effect on its own on MAP (88 ± 11 vs 85 ± 13 mm Hg; P = 1) and did not prevent adenosine in lowering MAP to a value similar to adenosine on its own (51 ± 4 mm Hg; P = 1 vs adenosine; P = 0.012 vs BnOCPA alone). CPA significantly decreased MAP (from 83 ± 8 to 51 ± 5 mm Hg; P = 0.017), a decrease that was not significantly different to the effect of adenosine in the absence or presence of BnOCPA (P = 1 for both). ns, not significant; **, P < 0.02; ***, P < 0.001; ****, P < 0.0001.

See also Figure S8.

Figure 6 BnOCPA is a potent analgesic without causing respiratory depression or sedation

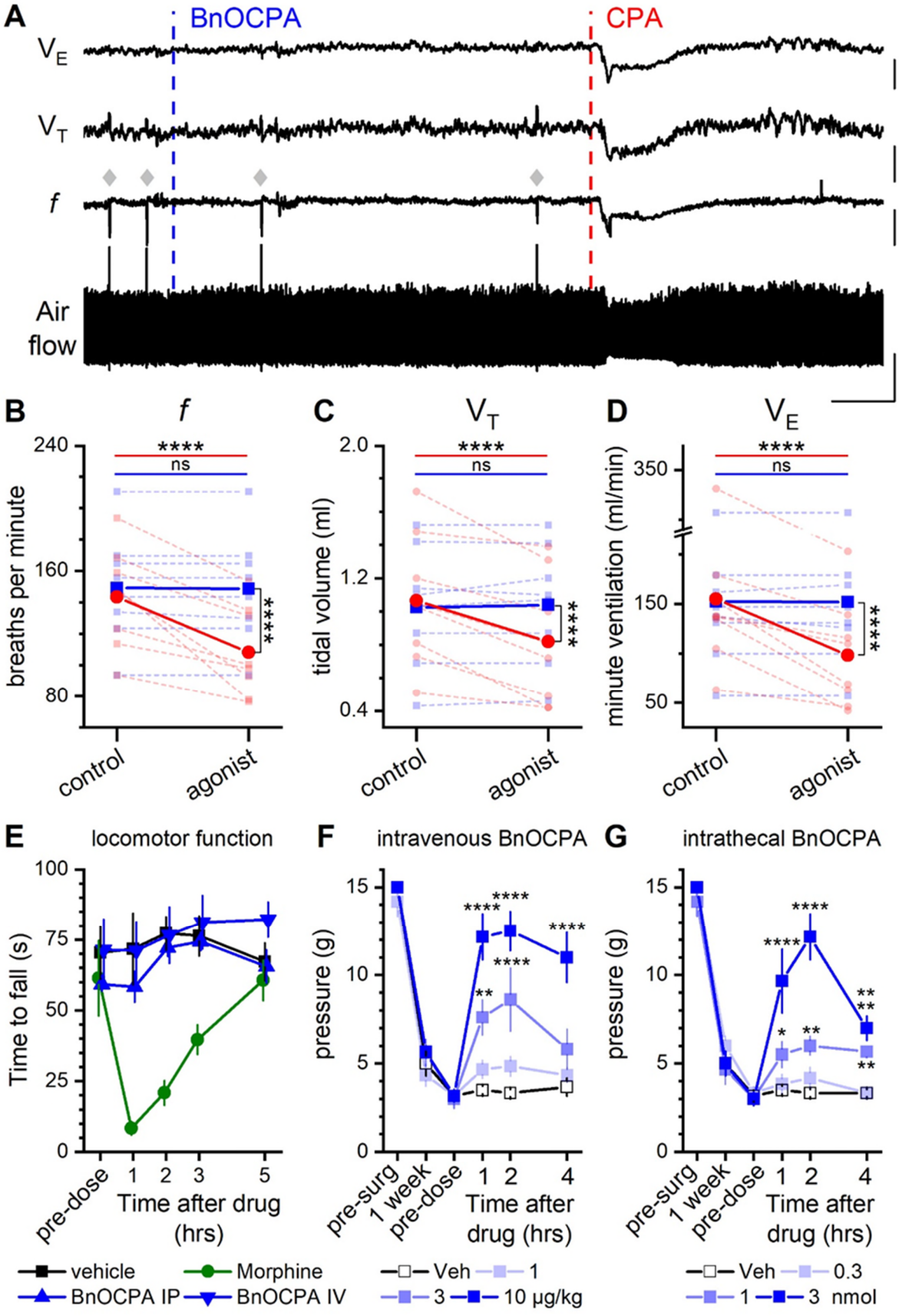

Figure 6 BnOCPA is a potent analgesic without causing respiratory depression or sedation

(A) examples of tracheal airflow, respiratory frequency (*f*), tidal volume (V_T) and minute ventilation (V_E) from a single urethane-anaesthetised, spontaneously breathing rat showing the lack of effect of BnOCPA on respiration and the respiratory depression caused by CPA. BnOCPA and CPA were given as a 350 µL·kg^{-1} IV bolus at the times indicated by the vertical broken lines (BnOCPA, 8.3 µg/kg, blue; CPA, 6.3 µg·kg^{-1}, red). Grey diamonds indicate spontaneous sighs. Scale bars measure: 180 s and: airflow, 0.5 mL; *f*, 50 breaths per minute (BrPM); V_T, 0.25 mL; V_E, 50 mL/min. **(B, C, D)** Summary data for 8 anaesthetised rats. Data from each rat is shown before and after the injection of BnOCPA (blue squares and broken lines) and CPA (red circles and broken lines) together with the mean value for all animals (solid lines) for *f*, V_T and V_E, respectively. One-way RM ANOVA: For: **B**, *f*, Greenhouse-Geisser corrected F(1.20, 8.38) = 30.4, P = 3.48 x 10^{-4}; **C**, V_T, F(3, 21) = 15.9, P = 1.25 x 10^{-5}, and **D**, V_E, Greenhouse-Geisser corrected F(1.19, 8.34) = 15.77, P = 0.003, with the following Bonferroni post hoc comparisons: Following BnOCPA, *f* (149 ± 12 BrPM), V_T (1.0 ± 0.1 mL), and V_E (152 ± 26 ml/min) were not altered (P = 1) compared to resting values *f* (149 ± 12 BPM), V_T (1.0 ± 0.1 mL), and V_E (152 ± 26). In contrast to CPA, which reduced *f* (108 ± 10 BrPM), V_T (0.8 ± 0.1 mL), and V_E (99 ± 19 ml/min) compared to resting values *f* (143 ± 11 BrPM; p = 4.05 x 10^{-6}), V_T (1.1 ± 0.1 mL; P = 2.58 x10^{-5}), and V_E (155 ± 28; P = 5.52 x 10^{-5}). Whilst the control resting values before administration of BnOCPA and CPA were not different to one another (P = 1). The effects of CPA were significantly greater than BnOCPA for *f* (P = 4.48 x 10^{-7}), V_T (P = 1.15 x10^{-4}), and V_E (P = 1.16 x10^{-4}). Horizontal significance indicators above the data show differences between resting values and following IV administration of either BnOCPA (blue line) or CPA (red line). Vertical significance indicators show differences between the effects of BnOCPA and CPA. **(E)** BnOCPA does not induce sedation or affect motor function. BnOCPA was administered IV (n = 6) or intraperitoneally (IP; n = 6) at 10 µg/kg as per the maximum dose used in the neuropathic pain study (Figure 6F). Morphine (n = 6) was administered at 15 mg/kg subcutaneously as a positive control for sedation and motor impairment. Saline (n = 6) was administered subcutaneously at the same volume as the morphine injection. Rats were tested on the rotarod over a period of 5 hours after injection. BnOCPA did not affect motor function at analgesic doses. Data points are presented as mean ± SEM and are offset for clarity. **(F, G)** BnOCPA alleviates mechanical allodynia in a spinal nerve

ligation (Chung) model of neuropathic pain when administered via an IV (**F**) or intrathecal (IT; **F**) route. Prior to surgery (pre-surg) animals had similar sensitivity to tactile stimulation as assessed by Von Frey hair stimulation. Spinal nerve ligation subsequently caused hypersensitivity to touch (mechanical allodynia) as evidenced by the reduction in the tactile pressure necessary to elicit paw withdrawal (paw withdrawal threshold; PWT) at 1 week after surgery. PWT reaches a similar nadir across all groups prior to vehicle or BnOCPA infusion (pre-dose). Administration of BnOCPA significantly increased PWT in the limb ipsilateral to the site of injury, in a dose-dependent manner (one-way ANOVA (pre-dose, 1, 2 and 4 hrs) for IV BnOCPA: $F(3,80) = 37.3$, $P = 3.44 \times 10^{-15}$; for IT BnOCPA $(3,76) = 47.0$, $P = 0$). Fisher LSD post-hoc comparisons showed significant differences at: IV 3 ug/kg at 1, 2 and 4 hrs, $P = 0.044$, 0.008 and 0.019, respectively, and 10 ug/kg at 1, 2 and 4 hrs, $P = 1.37 \times 10^{-8}$, 6.81×10^{-14} and 3.23×10^{-4}, respectively; IT 1 nmol at 1 and 2 hrs, $P = 0.001$ and 4.16×10^{-5}, respectively, and 10 nmol at 1, 2 and 4 hrs, $P = 9.52 \times 10^{-11}$, 1.42×10^{-11} and 1.41×10^{-8}, respectively. Averaged data (n = 6 per treatment, except for 1 nmol BnOCPA, n = 5) is presented as mean ± SEM. ns, not significant; ∗, $P < 0.05$; ∗∗, $P < 0.02$; ∗∗∗, $P < 0.001$; ∗∗∗∗, $P < 0.0001$.

Supplementary Data for:

A biased adenosine A_1R agonist confers analgesia without cardiorespiratory depression

Mark J. Wall, Emily Hill, Robert Huckstepp, Kerry Barkan, Giuseppe Deganutti, Michele Leuenberger, Barbara Preti, Ian Winfield, Haifeng Wei, Wendy Imlach, Eve Dean, Cherise Hume, Stephanie Hayward, Jess Oliver, Fei-Yue Zhao, David Spanswick, Christopher A. Reynolds, Martin Lochner, Graham Ladds and Bruno G. Frenguelli

Correspondence and requests for materials should be addressed to

Mark.Wall@warwick.ac.uk

Supplementary Figures S1 – S8

Supplementary Tables S1 – S3

Supplementary Movies S1 – S5

Supplementary References 1 - 3

Table S1 Human A_1R agonist binding and inhibition of cAMP production

	Human A_1R		
	Binding	cAMP inhibition	
	pK_i[a]	pIC_{50}[b]	Range[c]
Adenosine	5.02 ± 0.10	8.45 ± 0.2	55.7 ± 4.0
CPA	6.65 ± 0.14***	9.26 ± 0.3***	48.97 ± 0.7
NECA	6.45 ± 0.06***	9.05 ± 0.2***	34.33 ± 4.0
HOCPA	5.81 ± 0.16***	9.08 ± 0.1**	60.52 ± 1.5
BnOCPA	6.47 ± 0.11***	9.17 ± 0.3***	49.0 ± 0.66

Table S2 Binding affinities at rat A_1R, $A_{2A}R$ and A_3R

	Rat Adenosine Receptors		
	rA_1R pK_i[d]	$rA_{2A}R$ pK_i[d]	rA_3R pK_i[e]
Adenosine	5.41 ± 0.18	N.D	N.D
CPA	6.80 ± 0.14***	N.D	N.D
NECA	6.32 ± 0.13***	N.D	N.D
HOCPA	6.27 ± 0.14***	4.86 ± 0.12	6.17 ± 0.02
BnOCPA	6.25 ± 0.16**	5.03 ± 0.11	5.01 ± 0.12

Average data ± SEM of 4 - 19 individual replicates

[a] Negative logarithm of agonist concentration displacing 50% bound [^{3}H]-DPCPX

[b] Negative logarithm of agonist concentration producing half-maximal response

[c] Range of response observed upon agonist stimulation, as a percentage of response obtained upon stimulation with 10 μM forskolin

[d] Negative logarithm of agonist concentration displacing 50% bound CA200645

[e] Negative logarithm of agonist concentration displacing 50% bound AV039

Statistical difference between each agonist and adenosine was calculated using a one-way ANOVA with Dunnett's post-test (** $P < 0.01$; *** $P < 0.001$).

Related to Figures 1 and S4

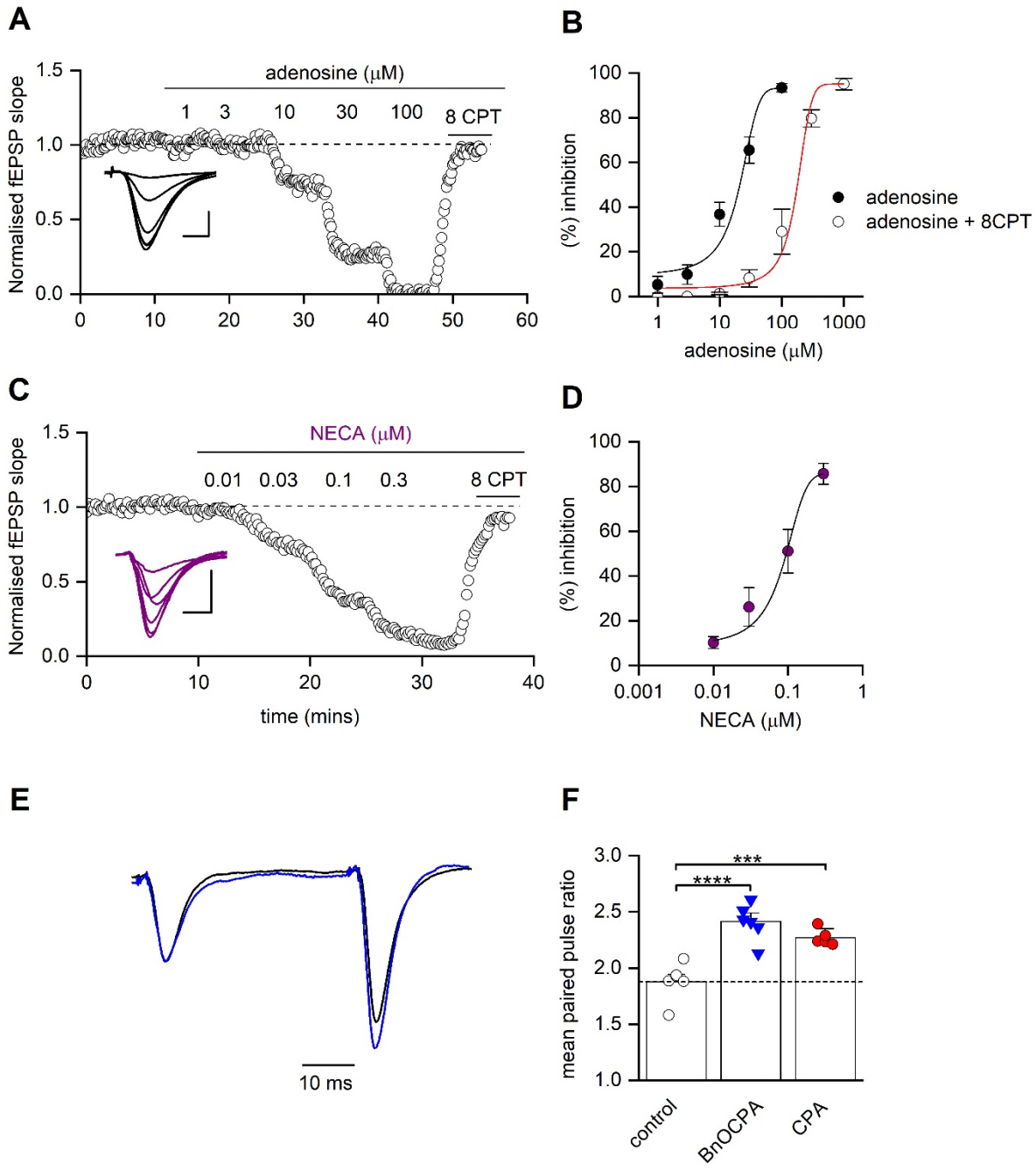

Figure S1. A_1R agonists inhibit excitatory synaptic transmission at hippocampal synapses.

(A), Increasing concentrations of adenosine reduced fEPSP slope, an effect reversed by the A_1R antagonist 8CPT (2 μM). Inset, superimposed fEPSP averages in control and in increasing concentrations of adenosine. Scale bar measures 5 ms and 0.25 mV. **(B)**, Concentration-response curve for adenosine (IC_{50} = 20 ± 4.3 μM, *n* =11 slices) and for adenosine with 2 μM 8CPT (IC_{50} = 125 ± 10 μM *n* = 5 slices). **(C)**, Increasing concentrations of the A_1R agonist NECA reduced fEPSP slope, an effect reversed by 8CPT (2 μM). Inset, superimposed fEPSP averages in control and in increasing concentrations of NECA. Scale

bar measures 5 ms and 0.25 mV. **(D)**, Concentration-response curve for NECA (IC_{50} = 8.3 ± 3 nM, *n* =11 slices). **(E)**, Example of average (5 traces) superimposed paired-pulse fEPSP waveforms (50 ms inter-pulse interval) in control (black trace) and in the presence of BnOCPA (100 nM; blue trace). The fEPSP waveforms have been normalised to the amplitude of the first fEPSP in control. BnOCPA increased paired-pulse facilitation, indicative of a BnOCPA-induced reduction in the probability of glutamate release. **(F)**, Data summary. For a paired-pulse interval of 50 ms, the paired-pulse ratio was significantly increased (one-way ANOVA; $F(2, 14) = 21.72$; $P = 5.11 \times 10^{-5}$) from 1.88 ± 0.07 in control (*n* = 6 slices) to 2.41 ± 0.07 in BnOCPA (*n* = 6 slices, $P = 5.17 \times 10^{-5}$) and 2.27 ± 0.03 in CPA (60 nM; *n* = 5, P = 0.001). Averaged data is presented as mean ± SEM. ***, P < 0.001; ****, P < 0.0001.

Related to Figure 1.

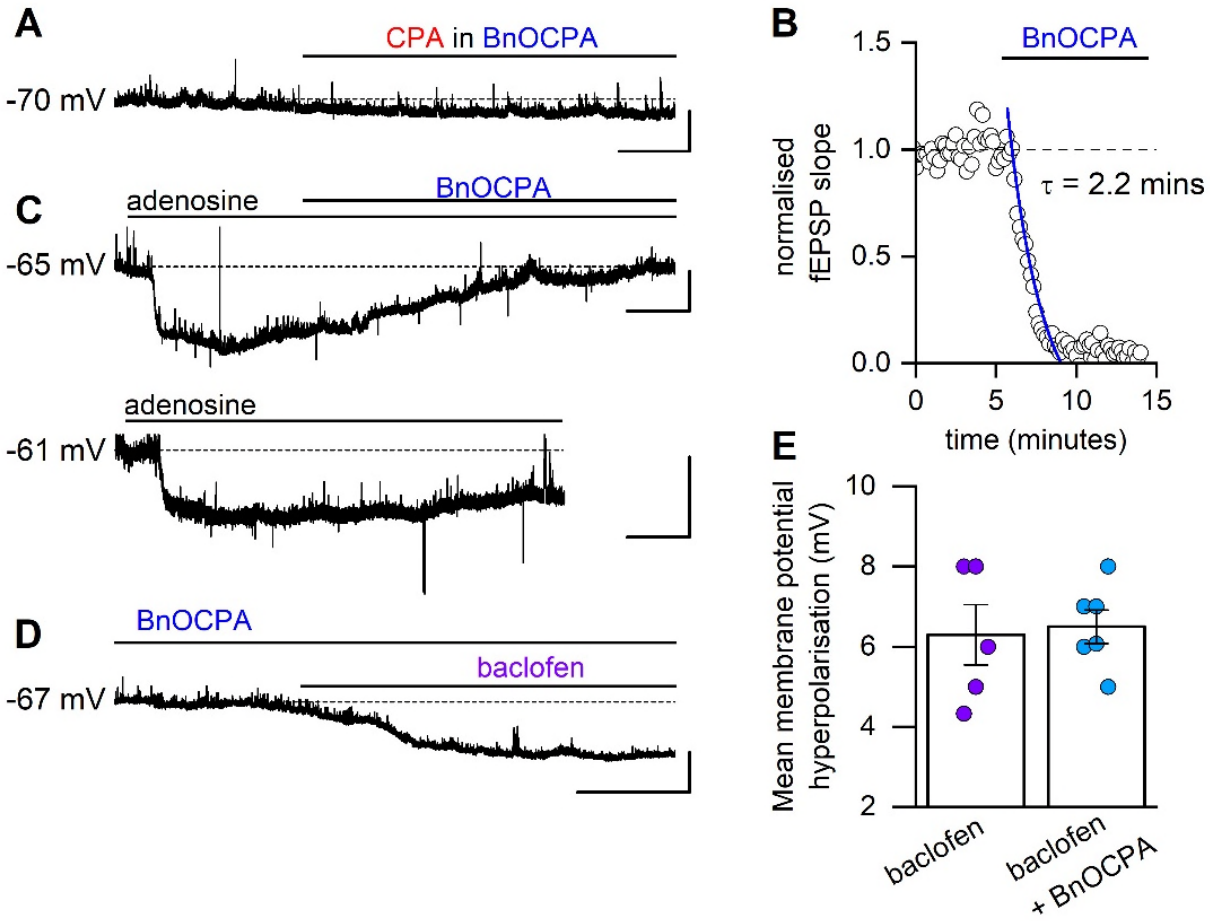

Figure S2. Selective action of BnOCPA on membrane hyperpolarisation induced by prototypical A_1R agonists versus that induced by the $GABA_B$ receptor agonist baclofen.

(A), Membrane potential trace recorded from a CA1 pyramidal cell. BnOCPA (300 nM) reduced the effect of CPA (300 nM; quantified in main text Figure 1H). **(B),** The same solution of BnOCPA (300 nM), which had no effect on membrane potential, abolished synaptic transmission in a sister slice (inhibition fitted with a single exponential; τ = 2.2 mins). **(C)**, BnOCPA reversed the hyperpolarising effect of adenosine (100 µM; similar observations were made in 3 other cells), which (lower trace) cannot be accounted for by fatigue of adenosine-mediated hyperpolarisation (similar observations of sustained hyperpolarisations to adenosine were made in 2 other cells). **(D)**, Application of baclofen (10 µM) in the presence of BnOCPA (300 nM) hyperpolarised the membrane potential (from -67 to -74 mV). Scale bars measure 5 mV and 50 s (CPA), 200 s (adenosine) or 100 s (baclofen). **(E)**, Data summary of baclofen/BnOCPA experiments. The mean hyperpolarisation produced by baclofen in the presence of BnOCPA was not significantly different (unpaired t-test) from that produced by baclofen in control conditions (6.5 ± 0.43 mV vs 6.3 ± 0.76 mV, P = 0.774, *n* = 5 - 6 cells for each condition). Bar chart displays individual data points and mean ± SEM.

Related to Figure 1.

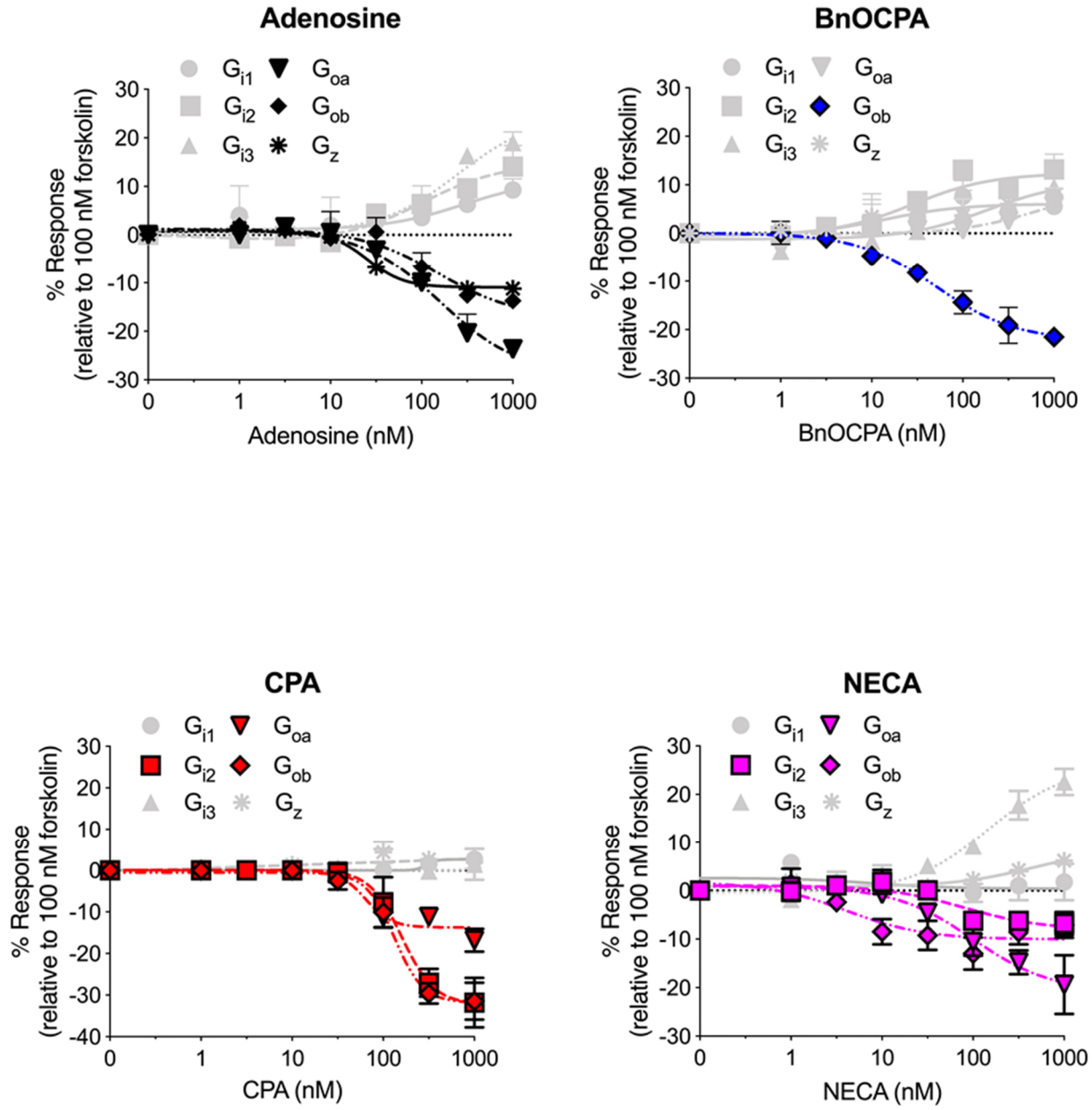

Figure S3. Prototypical and atypical A_1R agonists display differing Gαi/o activation profiles.

The ability of adenosine, BnOCPA, CPA and NECA to activate each individual Gi/o/z subtype was determined in CHO-K1-hA_1R cells, transfected with PTX-insensitive G proteins. cAMP levels were measured following 30 minute co-stimulation with 100 nM forskolin and each agonist. Adenosine displayed an ability to inhibit cAMP production via activation of Gi2, Goa, Gob, and Gz; CPA and NECA via Gi2, Goa and Gob, and BnOCPA exclusively via Gob. Data represented as the average level of cAMP production relative to that observed upon stimulation with 100 nM forskolin, ± SEM, of n = 4 - 6 individual replicates. Stimulation of cAMP production reflects activation of endogenous Gs by the A_1R and is in agreement with previous observations (Baker and Hill, 2007; Cordeaux et al., 2004; Hill and Baker, 2003).

Related to Figure 2.

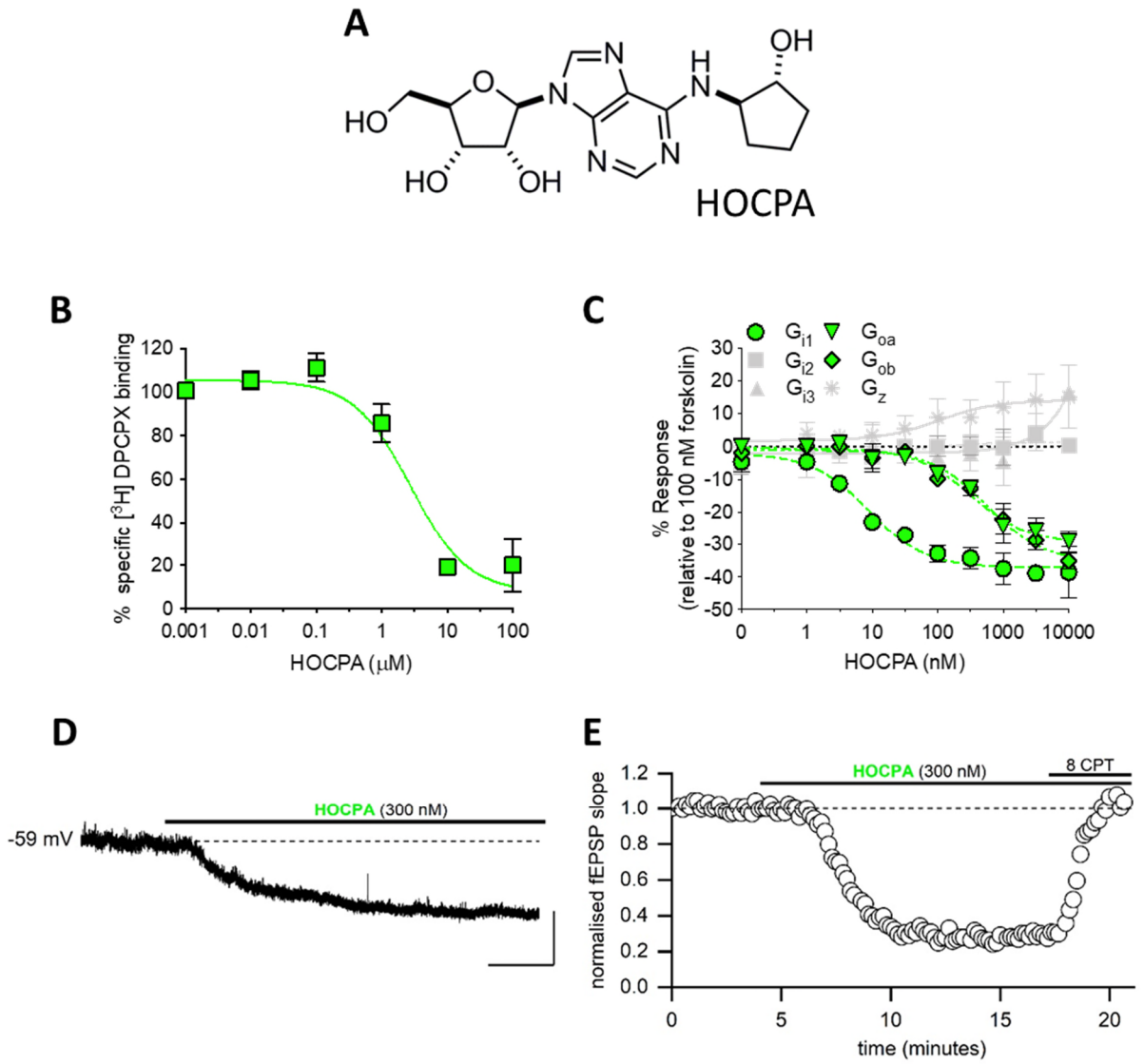

Figure S4. HOCPA does not show Gα signalling bias and does not discriminate between pre- and postsynaptic A_1Rs.

(A). Chemical structure of HOCPA. **(B)**, Binding of HOCPA was measured via its ability to displace [^{3}H]DPCPX from CHO-K1-hA_1R cells membranes. **(C)**, The ability of HOCPA to inhibit forskolin-stimulated (100 nM) cAMP production in PTX pre-treated (200 ng/ml) CHO-K1-hA_1R cells, transfected with PTX-insensitive Gi1, Gi2, Gi3, Goa, Gob or Gz. In contrast to BnOCPA, HOCPA shows no bias between Goa and Gob. All data are presented as mean ± SEM, of *n* = 4 - 5 individual replicates. **(D)**, Example membrane potential trace. HOCPA (300 nM) induced hyperpolarisation (mean hyperpolarisation 5.3 ± 0.5 mV, n = 6 cells). Scale bars measure 5 mV and 50 s. **(E)**, Graph plotting normalised fEPSP slope against time for a single experiment. HOCPA caused a ~80 % reduction in fEPSP slope, which was reversed by the A_1R antagonist 8CPT (4 μM). Similar results were observed in 4 slices.

Related to Figure 2.

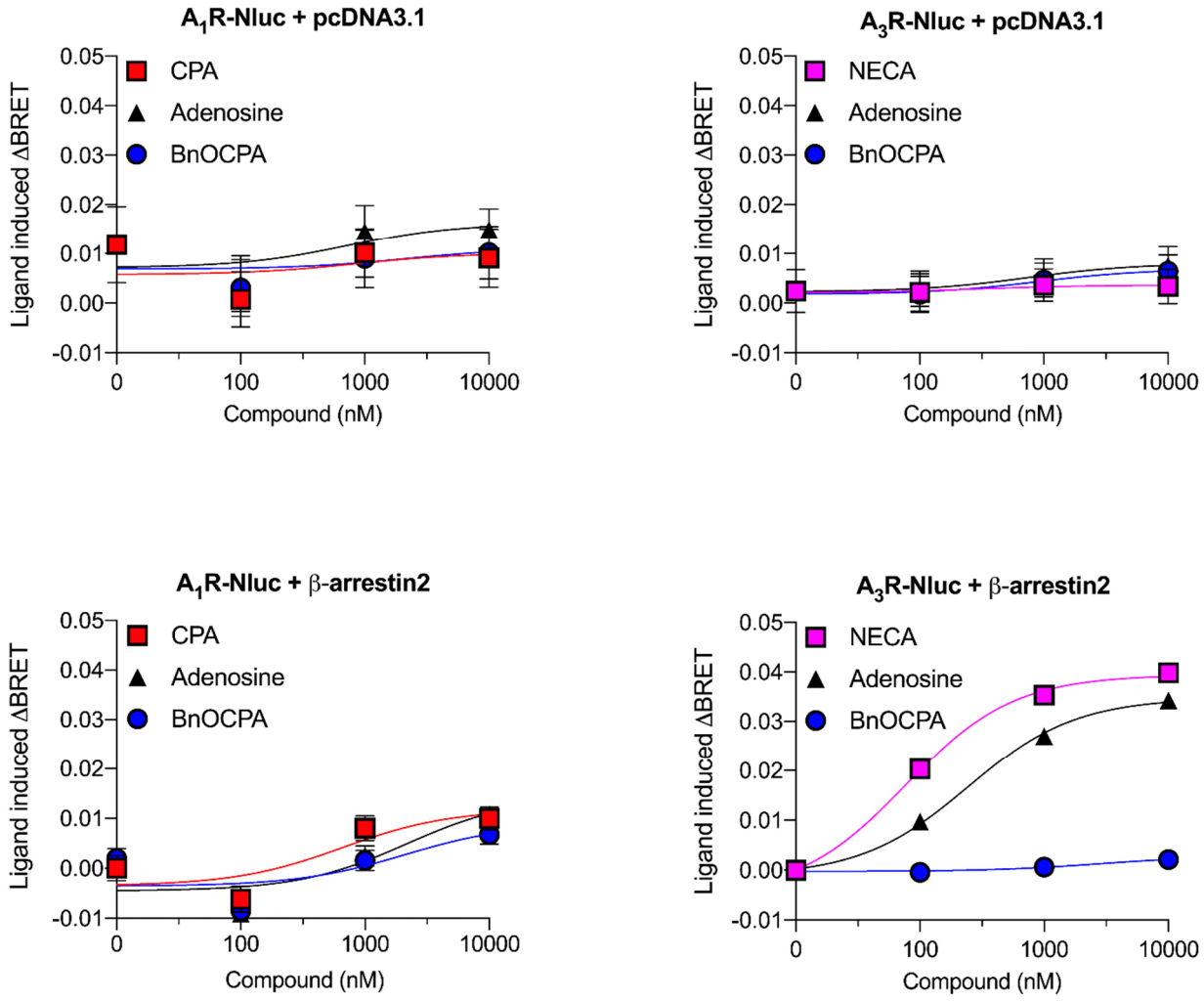

Figure S5. β-arrestin2 recruitment to the A_1R or A_3R.

Interaction was detected using BRET between a C-terminally tagged Nluc GPCR (A_1R or A_3R) and β-arrestin2 C-terminal tagged with Venus-YFP. Note lack of β-arrestin2 recruitment to the A_1R either by adenosine, CPA or BnOCPA, which yields BRET signals comparable to the vector control experiments (pcDNA3.1). A_3R recruitment of β-arrestin2 is provided as a positive control for the BRET assay.

Related to Figure 2.

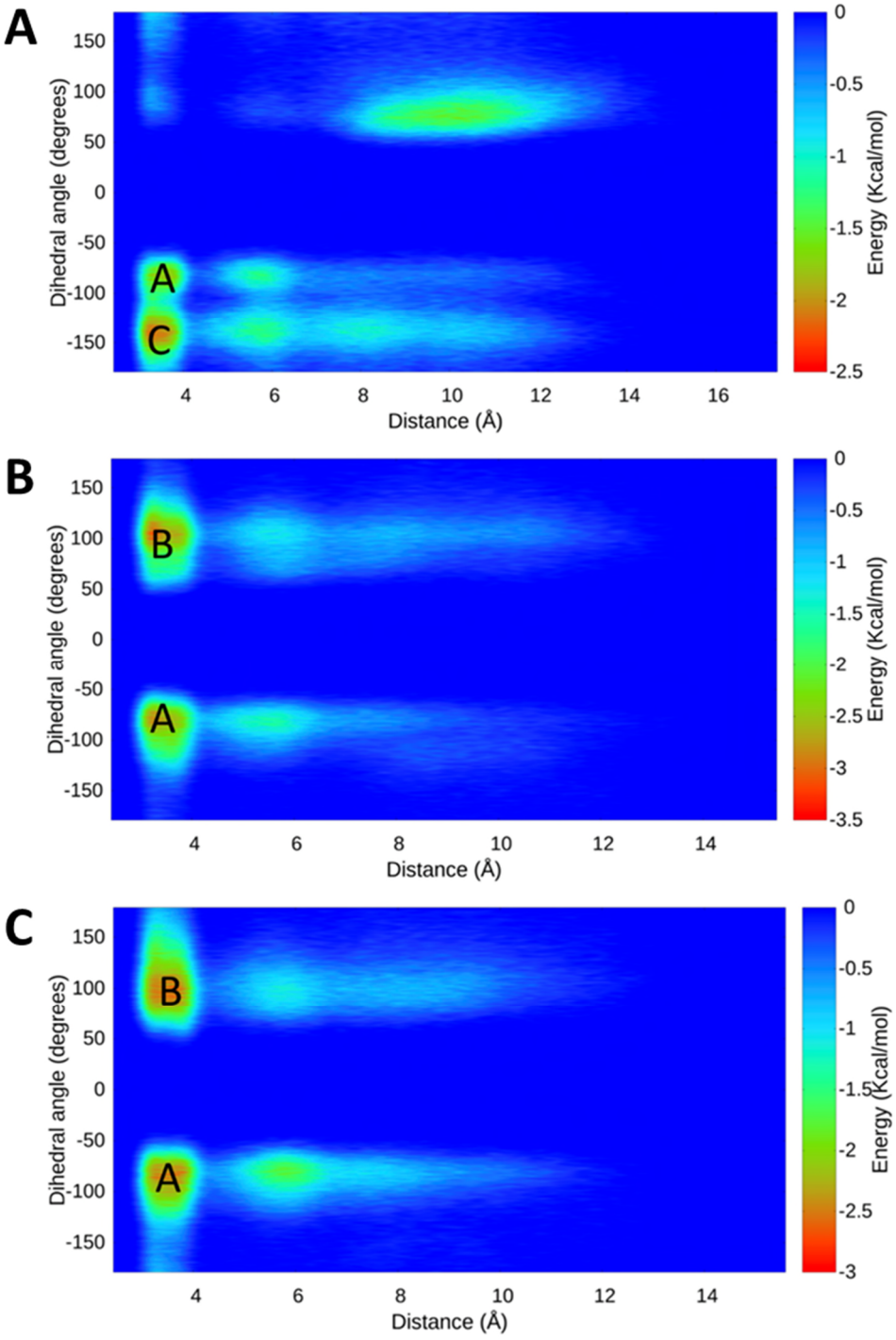

Figure S6. Energy surfaces obtained from metadynamics simulations of BnOCPA. Energy surface obtained by integrating the Gaussian terms deposited during three well-tempered metadynamics replicas (panels **A**, **B** and **C**). X axes report the distance between the E172^{ECL2} carboxyl carbon and the positively charged K265^{ECL3} nitrogen atom; Y axes indicate the dihedral angle formed by the 4 atoms linking BnOCPA cyclopentyl ring to the phenyl moiety. The three energy minima (A, B and C) correspond to the three binding modes proposed for BnOCPA (Modes A, B, C in Figure 3D to F, respectively).

Related to Figure 3.

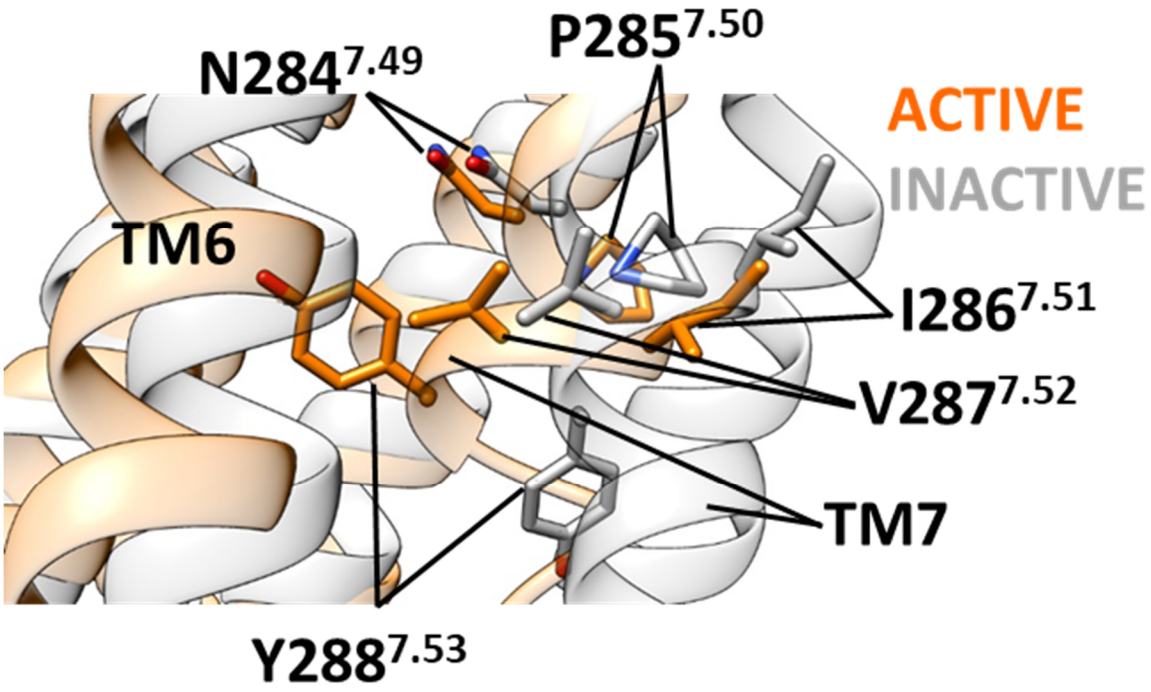

Figure S7. The conserved NPXXY motif ($N^{7.49}$ PIV $Y^{7.53}$) in the A_1R.

The root mean square deviation (RMSD) was computed with respect to the A_1R inactive conformation. Compared to the inactive conformation (grey), in the active state (orange) the distal portion of TM7 is moved towards the TM bundle core (which is responsible for G protein binding). Starting from the active conformation (orange) and in absence of bound G protein, simulations should allow the structure to partially relax towards the inactive state (grey) with a dynamic influenced by the orthosteric ligand.

Related to Figure 3.

Table S3. Transient hydrogen bonds between α4-β6 loop residue 317 (N317 in Goa, H317 in Gob), the α3-β5 loop residue D263, and the residue on H8 of the A_1R (Ballesteros Weinstein enumeration in superscript).

A_1R - Gα Interactions					
	Coupling Systems			**Non-coupling Systems**	
	Occupancy (%frames)			**Occupancy (%frames)**	
A_1R - Gα hydrogen bond	**BnOCPA mode D:Gob**	**BnOCPA mode B:Gob**	**HOCPA:Gob**	**BnOCPA mode D:Goa**	**BnOCPA mode B:Goa**
H317-Q293$^{8.48}$	**1.7**	**0.5**	**2.8**	**6.9**	**10.3**
D263-Q293$^{8.48}$	**0.4**	**0.4**	**1.5**	**9.2**	**0.6**
K294$^{8.49}$-D263	**0.0**	**0.0**	**0.1**	**4.0**	**2.9**
R296$^{8.51}$-D263	**0.1**	**0.5**	**0.0**	**10.7**	**0.0**

Related to Figure 4.

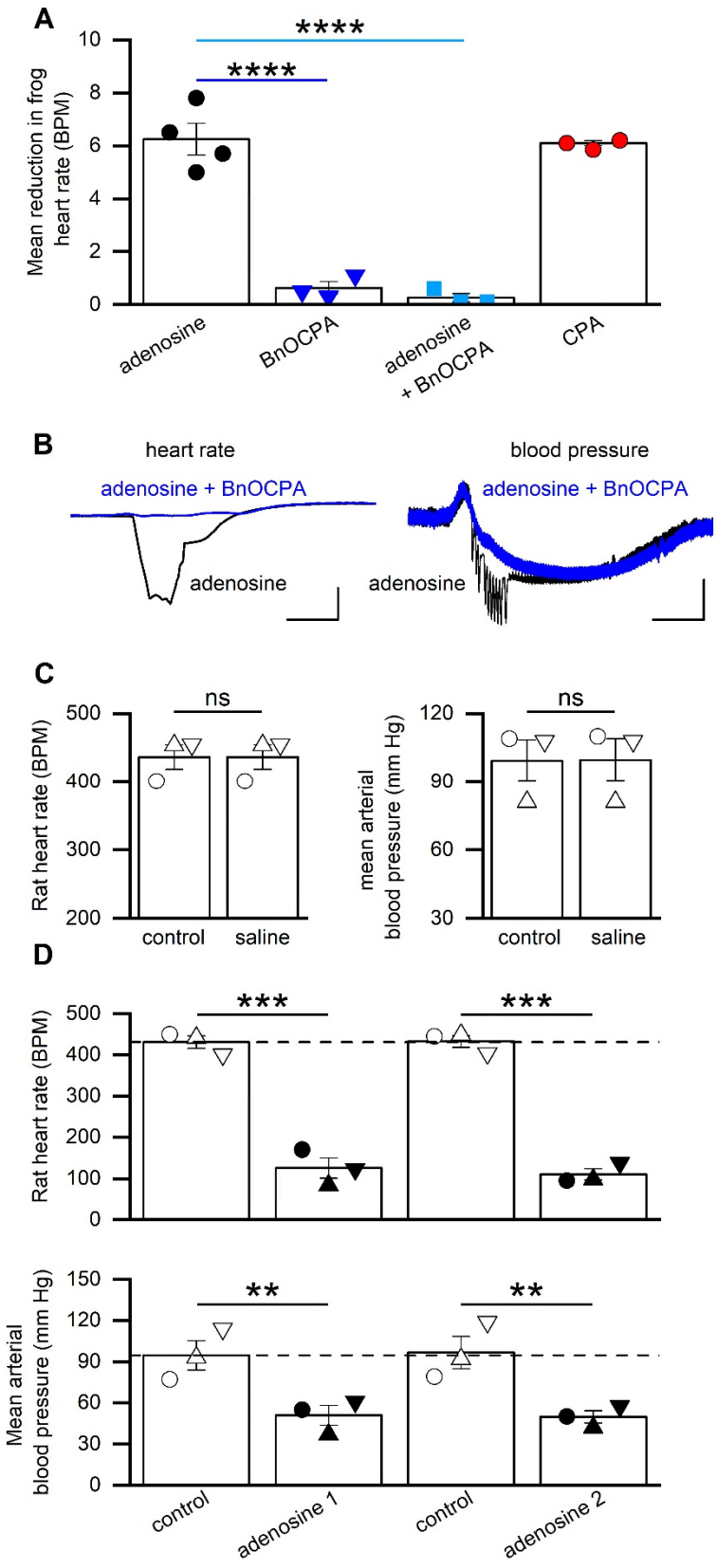

Figure S8. Actions of BnOCPA on frog heart rate and controls for anesthetised rat experiments.

Figure S8. Actions of BnOCPA on frog heart rate and controls for anesthetised rat experiments.

(A), Data summary for 3 - 4 isolated frog heart preparations. Application of adenosine (30 μM) reduced heart rate (HR) from 41.8 ± 1.3 BPM to 35.5 ± 1.3 BPM. BnOCPA (300 nM) had no effect on HR (42.8 ± 1.2 BPM vs 42.1 ± 1.2 BPM; change 0.6 ± 0.2 BPM), an effect that was significantly different from that of adenosine (blue line; $P = 2.22 \times 10^{-5}$). BnOCPA significantly (cyan line; $P = 1.31 \times 10^{-5}$) reduced the effects of subsequent adenosine applications (from a reduction of 6.3 ± 0.6 BPM to 0.3 ± 0.2 BPM). CPA (300 nM) reduced HR by 6.1 ± 0.1 BPM, a value similar to that of adenosine. One way ANOVA on the difference in HR across the 4 conditions ($F(3,9) = 64.64$; $P = 2.070 \times 10^{-6}$), with the reported Bonferroni-corrected P values. **(B)**, Representative traces from a urethane-anaesthetised, spontaneously breathing rat. BnOCPA blocks the effect of adenosine on heart rate (left traces), but only prevents the early phase of adenosine-induced hypotension (right trace). Data taken from the trace in Figure 5. Scale bars measure 100 BPM or 20 mm Hg and 6 s. **(C)**, Data summary for 3 urethane-anaesthetised, spontaneously breathing rats. Bar charts showing that injection of 0.9 % saline (equivalent volume to drug experiments) had no effect (paired t-test) on either HR (P = 1) or mean arterial blood pressure (MAP; P = 0.422). **(D)**, Data summary for 3 urethane-anaesthetised, spontaneously breathing rats. Repeated adenosine injections have the same significant effect on HR ($P = 1.40 \times 10^{-4}$ and 1.02×10^{-4}, respectively) and MAP (P = 0.012 and 0.008, respectively) and thus show no run down. One-way RM ANOVA for both HR (Greenhouse-Geisser corrected $F(1.97,3.94) = 96.79$, $P = 4.48 \times 10^{-4}$, and MAP ($F(1.10,2.20) = 19.46$, P = 0.040) from 3 animals. In **C** and **D**, each symbol represents data from a single rat. ns, not significant; **, P < 0.02; ***, P < 0.001; ****, P < 0.0001.

Related to Figure 5.

Supplementary Movies S1 - S5

Movie S1

Molecular dynamics dynamic docking simulation of BnOCPA binding to the apo A_1R
Extracellular (left) and orthogonal (right) views of BnOCPA (stick and transparent sphere representation) simulation of binding to the apo A_1R (white ribbon). Protein residues within 4 Å from the ligand atoms are shown (stick representation). Hydrogen bonds are highlighted as red dotted lines. Soon after it reached the orthosteric site, BnOCPA engaged $N254^{6.55}$ in a bi-dentate hydrogen bond. The ribose moiety, initially involved in an intramolecular hydrogen bond with the purine ring, interacts with side chains of internal residues, such as the key residue for receptor activation, $T277^{7.42}$. The benzyl moiety initially explores binding mode A, then moves to mode B (after about 720 ns).

Related to Figure 3.

Movie S2

Molecular dynamics dynamic docking simulation of HOCPA binding to the apo A_1R
Extracellular (left) and orthogonal (right) views of HOCPA (stick and transparent sphere representation) simulated binding to the apo A_1R (white ribbon). Protein residues within 4 Å from the ligand atoms are shown (stick representation). Hydrogen bonds are highlighted as red dotted lines. Soon after it entered into the orthosteric site, HOCPA engaged $N254^{6.55}$ in a bi-dentate hydrogen bond. In analogy to BnOCPA (Extended Data Movie 2) the ribose moiety, initially involved in an intramolecular hydrogen bond with the purine ring, interacts with side chains of inner located residues, such as the key residue for receptor activation $T277^{7.42}$. Further hydrogen bonds are formed between the cyclopentyl hydroxyl group and the ionic bridge between $E172^{ECL2}$ and $K265^{ECL3}$.

Related to Figure 3.

Movie S3

Molecular dynamics dynamic docking simulation of the Gob GαCT to the BnOCPA:A_1R complex. Intracellular view of the A_1R (white ribbon and transparent surface) during the binding simulations of Gob GαCT (also denoted as H5 – black ribbon). The transparent ribbon shows the position of the Gi2 GαCT as reported in the cryo-EM A_1R structure 6D9H. The supervision algorithm is switched off after about 43 ns of productive simulation.

Related to Figure 4.

Movie S4

Molecular dynamics simulation of the BnOCPA:A_1R:Goa(α subunit) complex. Intracellular view of the A_1R (white ribbon and cyan stick representation) bound to the Goa α subunit (orange ribbon and green stick representation) during one MD replica. After about 300 ns of simulation the system undergo a conformational transition characterized by transient hydrogen bonds between the receptor H8 (Q293$^{8.48}$ and R296$^{8.51}$) and the Goa residues located on the α3-β5 (D263) and α4-β6 (N317) loops.

Related to Figure 4.

Movie S5

Molecular dynamics simulation of the BnOCPA:A_1R:Gob(α subunit) complex. Intracellular view of the A_1R (white ribbon and cyan stick representation) bound to the Gob α subunit (orange ribbon and green stick representation) during one MD replica. The system shows lower flexibility than BnOCPA:A_1R:Goa. Stable interactions between the Gob α3-β5 loop and the α5 (GαCT) positively charged K347 and R350 occurs.

Related to Figure 4.

Supplementary Figures References

Baker, J.G., and Hill, S.J. (2007). A comparison of the antagonist affinities for the Gi- and Gs-coupled states of the human adenosine A1-receptor. J Pharmacol Exp Ther *320*, 218-228.

Cordeaux, Y., Ijzerman, A.P., and Hill, S.J. (2004). Coupling of the human A1 adenosine receptor to different heterotrimeric G proteins: evidence for agonist-specific G protein activation. Br J Pharmacol *143*, 705-714.

Hill, S.J., and Baker, J.G. (2003). The ups and downs of Gs- to Gi-protein switching. Br J Pharmacol *138*, 1188-1189.

Methods for:

A biased adenosine A_1R agonist confers analgesia without cardiorespiratory depression

Mark J. Wall, Emily Hill, Robert Huckstepp, Kerry Barkan, Giuseppe Deganutti, Michele Leuenberger, Barbara Preti, Ian Winfield, Haifeng Wei, Wendy Imlach, Eve Dean, Cherise Hume, Stephanie Hayward, Jess Oliver, Fei-Yue Zhao, David Spanswick, Christopher A. Reynolds, Martin Lochner, Graham Ladds and Bruno G. Frenguelli

Correspondence and requests for materials should be addressed to

Mark.Wall@warwick.ac.uk

Materials and Methods

Materials and Methods

Approvals. All experiments involving animals were conducted with the knowledge and approval of the University of Warwick Animal Welfare and Ethical Review Board, and in accordance with the U.K. Animals (Scientific Procedures) Act (1986) and the EU Directive 2010/63/EU. *In vivo* cardiorespiratory studies were conducted under the auspices of UK PPL 70/8936 and the chronic neuropathic pain studies under the auspices of P9D9428A9.

Preparation of hippocampal slices. Sagittal slices of hippocampus (300-400 μm) were prepared from male Sprague Dawley rats, at postnatal days 12-20 (Wall and Dale, 2013). Rats were kept on a 12-hour light-dark cycle with slices made 90 minutes after entering the light cycle. In accordance with the U.K. Animals (Scientific Procedures) Act (1986), rats were killed by cervical dislocation and then decapitated. The brain was removed, cut down the midline and the two sides of the brain stuck down to a metal base plate using cyanoacrylate glue. Slices were cut along the midline with a Microm HM 650V microslicer in cold (2-4°C) high Mg^{2+}, low Ca^{2+} aCSF, composed of (mM): 127 NaCl, 1.9 KCl, 8 $MgCl_2$, 0.5 $CaCl_2$, 1.2 KH_2PO_4, 26 $NaHCO_3$, 10 D-glucose (pH 7.4 when bubbled with 95% O_2 and 5% CO_2, 300 mOSM). Slices were stored at 34°C for 1-6 hours in aCSF (1 mM $MgCl_2$, 2 mM $CaCl_2$) before use.

Extracellular recording. A slice was transferred to the recording chamber, submerged in aCSF and perfused at 4-6 ml·min^{-1} (32 ± 0.5°C). The slice was placed on a grid allowing perfusion above and below the tissue and all tubing was gas tight (to prevent loss of oxygen). An aCSF-filled glass microelectrode was placed within stratum radiatum in area CA1 and recordings were made using either a differential model 3000 amplifier (AM systems, WA USA) or a DP-301 differential amplifier (Warner Instruments, Hampden, CT USA). Field excitatory postsynaptic potentials (fEPSPs) were evoked with either an isolated pulse stimulator model 2100 (AM Systems, WA) or ISO-Flex (AMPI, Jerusalem, Israel). For fEPSPs a 10-20 minute baseline was recorded at a stimulus intensity that gave 40-50% of the maximal response. Signals were acquired at 10 kHz, filtered at 3 kHz and digitised on line (10 kHz) with a Micro CED (Mark 2) interface controlled by Spike software (Vs 6.1, Cambridge Electronic Design, Cambridge UK) or with WinLTP (Anderson and Collingridge, 2007).

For fEPSP slope, a 1 ms linear region after the fibre volley was measured. Extracellular recordings were made independently on two electrophysiology rigs. As the data obtained from each rig was comparable both sets of data have been pooled.

Seizure model. Seizure activity was induced in hippocampal slices using nominally Mg^{2+}-free aCSF that contained no added Mg^{2+} and with the total K^+ concentration increased to 6 mM with KCl. Removal of extracellular Mg^{2+} facilitates depolarisation via glutamate N-methyl-D-aspartate (NMDA) receptor activation. Increasing the extracellular concentration of K^+ depolarises neurons leading to firing and release of glutamate to sustain activity. Both the increase in K^+ concentration and removal of Mg^{2+} are required to produce spontaneous activity in hippocampal slices (Frenguelli and Wall, 2016). Spontaneous activity was measured with an aCSF-filled microelectrode placed within stratum radiatum in area CA1.

Whole-cell patch clamp recording from hippocampal pyramidal cells. A slice was transferred to the recording chamber and perfused at 3 ml·min^{-1} with aCSF at 32 ± 0.5°C. Slices were visualized using IR-DIC optics with an Olympus BX151W microscope (Scientifica) and a CCD camera (Hitachi). Whole-cell current- and voltage-clamp recordings were made from pyramidal cells in area CA1 of the hippocampus using patch pipettes (5–10 MΩ) manufactured from thick walled glass (Harvard Apparatus, Edenbridge UK) and containing (mM): potassium gluconate 135, NaCl 7, HEPES 10, EGTA 0.5, phosphocreatine 10, MgATP 2, NaGTP 0.3 and biocytin 1 mg ml^{-1} (290 mOSM, pH 7.2). Voltage and current recordings were obtained using an Axon Multiclamp 700B amplifier (Molecular Devices, USA) and digitised at 20 KHz. Data acquisition and analysis was performed using Pclamp 10 (Molecular Devices, USA). For voltage clamp experiments, CA1 pyramidal cells were held at -60 mV. Peptides to interfere with G protein signalling were introduced via the patch pipette into the recorded cell. The cell was held for at least 10 minutes before adenosine (10 μM) was added to induce an outward current.

Frog heart preparation. Young adult male *Xenopus leavis* frogs were obtained from Portsmouth Xenopus Resource Centre. Frogs were euthanized with MS222 (0.2 % at a pH of 7), decapitated and pithed. The animals were dissected to reveal the heart and the pericardium was carefully

removed. Heart contractions were measured with a force transducer (AD instruments). Heart rate was acquired via a PowerLab 26T (AD instruments) controlled by LabChart 7 (AD instruments). The heart was regularly washed with Ringer solution and drugs were applied directly to the heart.

***In vivo* anaesthetised rat preparation for cardiorespiratory recordings:** Anaesthesia was induced in adult male Sprague Dawley rats (230-330 g) with isofluorane (2-4%; Piramal Healthcare). The femoral vein was catheterised for drug delivery. Anaesthesia was maintained with urethane (1.2-1.7 $g \cdot kg^{-1}$; Sigma) in sterile saline delivered via the femoral vein catheter. Body temperature was maintained at 36.7°C via a thermocoupled heating pad (TCAT 2-LV; Physitemp). The trachea was cannulated and the femoral artery catheterised, and both were connected to pressure transducers (Digitimer) to record respiratory airflow and arterial blood pressure, respectively. Blood pressure and airflow signals were amplified using the NeuroLog system (Digitimer) connected to a micro1401 interface and acquired on a computer using Spike2 software (Cambridge Electronic Design). Arterial blood pressure recordings were used to derive heart rate (HR: $beats.minute^{-1}$; BPM), and to calculate mean arterial blood pressure (MAP: Diastolic pressure + ⅓*[Systolic Pressure - Diastolic pressure]). Airflow measurements were used to calculate: tidal volume (V_T; mL; pressure sensors were calibrated with a 3 mL syringe), and respiratory frequency (*f*; $breaths \cdot min^{-1}$; BrPM). Minute ventilation (V_E; $mL \cdot min^{-1}$) was calculated as $f \times V_T$.

Cardiovascular and respiratory parameters were allowed to stabilise before experiments began. , A_1R agonists were administered by intravenous (IV) injection and the changes in HR, MAP, *f*, V_T, and V_E were measured. In pilot studies, the optimal dose of adenosine was determined by increasing the dose until robust and reliable changes in HR and MAP were produced (1 $mg \cdot kg^{-1}$). The dose of CPA was adjusted until equivalent effects to adenosine were produced on HR and MAP (6.3 $\mu g \cdot kg^{-1}$). For BnOCPA we initially used 5 $\mu g \cdot kg^{-1}$, but saw no agonist effect on HR and MAP. To ensure this was not a false negative we increased the dose of BnOCPA (8.3 $\mu g \cdot kg^{-1}$), which still gave no agonist effect on HR and MAP. However, as BnOCPA produced an antagonistic effect when co-administered with adenosine (Figure 5; Figure S8B), it must have reached A_1Rs at a high enough concentration to be physiologically active. These observations confirmed that the lack of agonistic

effects on HR and MAP were not due to a type II error. 8.3 μg·kg^{-1} BnOCPA was used for all further experiments. All injections were administered IV as a 350 μl·kg^{-1} bolus.

In the experimental study, rats received an injection of adenosine. After cardiorespiratory parameters returned to baseline (5-10 minutes) rats were given BnOCPA. After allowing sufficient time for any effect of BnOCPA to be observed, rats received adenosine with BnOCPA co-administered in a single injection. After cardiorespiratory parameters returned to baseline, rats were injected with CPA.

To check that the volume of solution injected with each drug did not itself induce a baroreflex response leading to spurious changes in cardiorespiratory responses, equivalent volumes of saline (0.9 %) were injected. These had no effect on either heart rate or MAP (Figure S8C). To confirm that repeated doses of adenosine produced the same response and that the responses did not run-down, rats were given two injections of adenosine (1 mg·kg^{-1}). There was no significant difference in the changes in cardiovascular parameters produced by each adenosine injection (Figure S8D).

An additional series of experiments (n = 4) were undertaken to directly compare BnOCPA and CPA on respiration. Adult male Sprague Dawley rats (400-500 g) were anaesthetised with urethane and instrumented as described above, with the exception that the arterial cannulation was not performed.

After allowing the animal to stabilise following surgery, BnOCPA (8.3 μg·kg^{-1}) was administered. After a 20 minutes recovery period CPA (6.3 μg·kg^{-1}) was administered. All injections were administered IV as a 350 μl·kg^{-1} bolus. Changes in *f*, V_T, and V_E were measured. If the dosing occurred close to a respiratory event such as a sigh a second IV dose was administered, with 20 minute recovery periods either side of the injection. Measurements for the effect of BnOCPA were time-matched to when CPA induced a change in respiration in the same preparation. As no difference was observed between the respiratory responses to BnOCPA in these rats (n = 4) and those instrumented for both cardiovascular and respiratory recordings (n = 4), the data were pooled (n = 8; Figure 6A to D).

Spinal nerve ligation (Chung model (Kim and Chung, 1992)): Adult male Sprague-Dawley rats, 7-8 weeks old, weighing around 250 g at the time of Chung model surgery, were purchased from Charles River UK Ltd. The animals were housed in groups of 4 in an air-conditioned room on a 12-

hour light/dark cycle. Food and water were available *ad libitum*. They were allowed to acclimatise to the experimental environment for three days by leaving them on a raised metal mesh for at least 40 min. The baseline paw withdrawal threshold (PWT) was examined using a series of graduated von Frey hairs (see below) for 3 consecutive days before surgery and re-assessed on the 6th to 8th day after surgery and on the 13th to 17th day after surgery before drug dosing.

Prior to surgery each rat was anaesthetized with 3% isoflurane mixed with oxygen (2 L·min^{-1}) followed by an i.m. injection of ketamine (60 mg·kg^{-1}) plus xylazine (10 mg·kg^{-1}). The back was shaved and sterilized with povidone-iodine. The animal was placed in a prone position and a para-medial incision was made on the skin covering the L4-6 level. The L5 spinal nerve was carefully isolated and tightly ligated with 6/0 silk suture. The wound was then closed in layers after a complete hemostasis. A single dose of antibiotics (Amoxipen, 15 mg/rat, i.p.) was routinely given for prevention of infection after surgery. The animals were placed in a temperature-controlled recovery chamber until fully awake before being returned to their home cages. The vehicle (normal saline) was administered via the intravenous (IV) route at 1 ml·kg^{-1} and via the intrathecal (IT) route at 10 µl for each injection. The rats with validated neuropathic pain state were randomly divided into 8 groups: vehicle IV, BnOCPA at 1, 3, 10 µg·kg^{-1} g IV; vehicle IT, BnOCPA at 0.3, 1, and 3 nmol IT groups.

To test for mechanical allodynia the animals were placed in individual Perspex boxes on a raised metal mesh for at least 40 minutes before the test. Starting from the filament of lower force, each filament was applied perpendicularly to the centre of the ventral surface of the paw until slightly bent for 6 seconds. If the animal withdrew or lifted the paw upon stimulation, then a hair with force immediately lower than that tested was used. If no response was observed, then a hair with force immediately higher was tested. The highest value was set at 15 g. The lowest amount of force required to induce reliable responses (positive in 3 out of 5 trials) was recorded as the value of PWT. On the testing day, PWT were assessed before and 1, 2 and 4 hours following BnOCPA or vehicle administration. The animals were returned to their home cages to rest (about 30 min) between two neighbouring testing time points. At the end of each experiment, the animals were deeply anaesthetised with isoflurane and killed by decapitation.

Rotarod test for motor function. A rotarod test was used to assess motor coordination following intravenous and intraperitoneal administration of BnOCPA. An accelerating rotarod (Ugo Basile) was set so speed increased from 6 to 80 rpm over 170 seconds. Male Sprague Dawley rats (n = 24), 7 weeks of age (212-258g) were trained on the rotarod twice daily for two days (≥2 trials per session) until performance times were stable. On the day of the experiment, three baseline trials were recorded. The compound was administered IP or intravenously via tail vein injection (10 µg/kg, n = 6 per group). The control group received subcutaneous saline and the positive control group received subcutaneous morphine (15 mg/kg). Latency to fall (seconds) was measured in triplicate at 1, 2, 3 and 5 hours post drug administration.

Cell signaling assays. CHO-K1-hA_1R cells were routinely cultured in Hams F12 nutrient mix supplemented with 10% Foetal bovine serum (FBS), at 37°C with 5% CO_2, in a humidified atmosphere. For cAMP inhibition experiments, cells were seeded at a density of 2000 cells per well of a white 384-well optiplate and co-stimulated, for 30 minutes, with 1 µM forskolin and a range of agonist concentrations (1 µM – 1 pM). cAMP levels were then determined using a LANCE® cAMP kit as described previously (Knight et al., 2016; Weston et al., 2016).

For determination of individual $G\alpha_{i/o/z}$ couplings, CHO-K1-hA_1R cells were transfected with pcDNA3.1-GNAZ or, pcDNA3.1 containing pertussis toxin (PTX) insensitive $G\alpha_{i/o}$ protein mutants (C351I, C352I, C351I, C351I, C351I, for G_{i1}, G_{i2}, G_{i3}, G_{oa}, G_{ob}, respectively, obtained from cDNA Resource Center; www.cdna.org), using 500 ng plasmid and Fugene HD at a 3:1 (Fugene:Plasmid) ratio. Cells were then incubated for 24 hours before addition of 100 ng/ml PTX, to inhibit activity of endogenous $G\alpha_{i/o}$, and then incubated for a further 16-18 hours. Transfected cells were then assayed as per cAMP inhibition experiments, but co-stimulated with agonist and 100 nM forskolin.

β-arrestin recruitment assays. HEK 293 cells were routinely grown in DMEM/F-12 GlutaMAX™ (Thermo Fisher Scientific) supplemented with 10% foetal bovine serum (FBS) (F9665, Sigma-Aldrich) and 1x antibiotic-antimycotic (Thermo Fisher Scientific) (DMEM complete). For analysis of β-arrestin2 recruitment following ligand stimulation at the human A_1R or A_3R, HEK 293 cells in a

single well of 6-well plate (confluency ≥80%) were transiently co-transfected with either A_1R-Nluc or A_3R-Nluc and β-arrestin2-YFP (total 2 µg, at a 1:6 ratio) using polyethyleneimine (PEI, 1 mg/ml, MW = 25,000 g/mol) (Polysciences Inc) at a DNA:PEI ratio of 1:6 (w/v). Briefly, in sterile tubes containing 150 mM sodium chloride (NaCl), DNA or PEI was added (final volume 50 µl), allowed to incubate at room temperature for 5 minutes, mixing together and incubating for a further 10 minutes prior to adding the combined mix dropwise to the cells. 24 hours post-transfection, HEK 293 cell were harvested, resuspended in reduced serum media (MEM, NEAA (Thermo Fisher Scientific) supplemented with 1% L-glutamine (2 mM final) (Thermo Fisher Scientific), 2% FBS and 1x antibiotic-antimycotic) and seeded (50,000 cells/well) in a poly-L-lysine-coated (MW 150,000-300,000, Sigma-Aldrich) white 96-well plate (PerkinElmer Life Sciences). 24 hours post seeding, media was removed, cells gently washed in PBS and 90 µl of furimazine (4 µM) containing solution added (PBS supplemented with 0.49 mM $MgCl_2$, 0.9 mM $CaCl_2$ and 0.1% BSA) to each well before incubating in the dark for 10 minutes. After incubation, 10 µl of ligand (NECA/CPA, adenosine, BnOCPA) was added in the range of 10 µM to 0.01 µM and filtered light emission measured at 450 nm and 530 nm every minute for 1 hour using a Mithras LB 940 (Berthold technology). Here, Nluc on the C-terminus of A_1R or A_3R acted as the BRET donor (luciferase oxidizing its substrate) and YFP acted as the fluorescent acceptor. Vehicle control (DMSO) was added to determine background emission.

Radioligand binding. Radioligand displacement assays were conducted using crude membrane preparations (100 µg protein per tube) acquired from homogenisation of CHO-K1-hA_1R cells in ice-cold buffer (2 mM $MgCl_2$, 20 mM HEPES, pH 7.4). The ability to displace binding of the A_1R selective antagonist radioligand, 1,3-[^{3}H]-dipropyl-8-cyclopentylxanthine ([^{3}H]-DPCPX) at a concentration (1 nM) around the Kd value (1.23 nM, as determined by saturation binding experiments) by increasing concentrations of NECA, adenosine, CPA, BnOCPA or HOCPA (10 µM – 0.1 nM) allowed the binding affinities (Ki) to be determined. Non-specific binding was determined in the presence of 10 µM DPCPX. Membrane incubations were conducted in Sterilin™ scintillation vials (Thermo Fisher Scientific; Wilmington, Massachusetts, USA) for 60 minutes at room temperature. Free radioligand was separated from bound radioligand by filtration through Whatman® glass microfiber GF/B 25 mm

filters (Sigma-Aldrich). Each filter was then placed in a Sterilin™ scintillation vial and radioactivity determined by: addition of 4 mL of Ultima Gold XR liquid scintillant (PerkinElmer), overnight incubation at room temperature and the retained radioactivity determined using a Beckman Coulter LS 6500 Multi-purpose scintillation counter (Beckman Coulter Inc.; Indiana, USA).

NanoBRET ligand-binding studies. Real-time pharmacological interactions between ligands and receptors was quantitated using NanoBRET as described previously (Barkan et al., 2019). In brief, using N-terminally NanoLuc (Nluc)-tagged rat A_1R, $A_{2A}R$ and A_3R expressing HEK-293 cell lines, competition binding assays were conducted. The data was fitted with the 'one-site – Ki model' derived from the Cheng and Prusoff correction (Cheng and Prusoff, 1973), built into Prism to determine affinity (pK_i) values for all unlabelled agonists at all adenosine receptor subtypes assayed. In all cases CA200645, which acts as a fluorescent antagonist with a slow off-rate (Stoddart et al., 2012) was used with the exception of the rat A_3R where the fluorescent compound was AV039 (Vernall et al., 2012). For all adenosine receptors filtered light emission at 450 nm and > 610 nm (640-685 nm band pass filter) was measured using a Mithras LB 940 and the raw BRET ratio calculated by dividing the 610 nm emission with the 450 nm emission. The Nluc acts as the BRET donor (luciferase oxidizing its substrate) and CA200645/AV039 acted as the fluorescent acceptor. CA200645 was used at 25 nM, as previously reported (Stoddart et al., 2015) and AV039 was used at 100 nM (Barkan et al. 2019). BRET was measured following the addition of the Nluc substrate, furimazine (0.1 μM). Nonspecific binding was determined using a high concentration of unlabelled antagonist, DPCPX for rat A_1R, ZM241385 for the rat $A_{2A}R$ and MRS 1220 for rat A_3R.

Data Analysis. Concentration-response curves for the effects of A_1R agonists on synaptic transmission were constructed in OriginPro 2018 (OriginLab; Northampton, MA, USA) and fitted with a logistic curve using the Levenberg Marquadt iteration algorithm. OriginPro 2018 was also used for statistical analysis. Statistical significance was tested as indicated in the text using paired or unpaired t-tests or one-way or two-way ANOVAs with repeated measures (RM) as appropriate. Bonferroni corrections for multiple comparisons were performed. All *in vitro* cell signalling assay data was analysed using Prism 8.4 (Graphpad software, San Diego, CA), with all concentration-response curves being fitted using a 3 parameter logistic equation to calculate response range and IC_{50}. All

cAMP data was normalised to a forskolin concentration-response curve ran in parallel to each assay. Where appropriate the operational model of receptor agonism (Black and Leff, 1983; Weston et al., 2016) was used to obtain efficacy (log τ) and equilibrium disassociation constant (log K_A) values. Calculation of bias factors ($\Delta\log(Tau/K_A)$) relative to adenosine was performed as described in Weston *et al.* (2016). Error for this composite measure was propagated by applying the following equation.

$$Pooled\ SEM = \sqrt{\left(\frac{SEM_A}{\overline{x}_A}\right)^2 + \left(\frac{SEM_B}{\overline{x}_B}\right)^2} \times \overline{x}_{AB}$$

Where, σ_A and σ_B are the standard deviations of measurement A and B with mean of $\overline{x}_A$ and $\overline{x}_B$, $\overline{x}_{AB}$ is the composite mean and n is the number of repeats.

Statistical significance to adenosine was calculated using a one-way ANOVA with a Dunnett's post-test for multiple comparisons. Radioligand displacement curves were fitted to the one-site competition binding equation yielding logKi values. One-way ANOVA (Dunnett's post-test) was used to determine significance by comparing the logKi value for each compound when compared to adenosine. To determine the extent of ligand-induced recruitment of β-arrestin2-YFP to either the A_1R or A_3R, the BRET signal was calculated by subtracting the 530 nm/450 nm emission for vehicle-treated cells from ligand-treated cells (ligand-induced ΔBRET). ΔBRET for each concentration at 5 minutes (maximum response) was used to produce concentration-response curves.

All *in vivo* cardiovascular and respiratory data were analysed using OriginPro 2018. One-way ANOVAs, with repeated measures as appropriate, and with Bonferroni correction for multiple comparisons were used. Statistical significance for the effects of IV saline was tested using paired t-tests. Data are reported throughout as mean ± SEM and n values are reported for each experiment. For the neuropathic pain studies, one-way ANOVAs with Fisher's Least Significant Difference (LSD) post-hoc test was used to compare drug treatment groups to the vehicle group (OriginPro 2018). The significance level was set at $P < 0.05$, with actual P values reported in the figure legends and summaries, by way of abbreviations and asterisks, on the graphs: ns, not significant; ∗ $P < 0.05$; ∗∗, $P < 0.02$; ∗∗∗, $P < 0.001$; ∗∗∗∗, $P < 0.0001$.

Drugs and substances. Drugs were made up as stock solutions (1-10 mM) and then diluted in aCSF or saline on the day of use. BnOCPA (Jagtap, 2011) ((2*R*,3*R*,4*S*,5*R*)-2-(6-{[(1*R*,2*R*)-2-benzyloxycyclopentyl]amino}-9*H*-purin-9-yl)-5-(hydroxymethyl)oxolane-3,4-diol) and HOCPA (Evans, 1989) ((2*R*,3*R*,4*S*,5*R*)-2-(6-{[(1*R*,2*R*)-2-hydroxycyclopentyl]amino}-9*H*-purin-9-yl)-5-(hydroxymethyl)oxolane-3,4-diol), the [(1*R*,2*R*)-2-hydroxycyclopentyl]amino bis-epimer of known A_1R agonist GR79236 (Strong et al., 1993), were synthesised as described previously (Knight et al., 2016) and dissolved in dimethyl-sulphoxide (DMSO, 0.01% final concentration). Adenosine, 8-CPT (8-cyclopentyltheophylline), NECA (5′-(*N*-Ethylcarboxamido) adenosine) and CPA (*N*^{6}-Cyclopentyladenosine) were purchased from Sigma-Aldrich (Poole, Dorset, UK). 1,3-[^{3}H]-dipropyl-8-cyclopentylxanthine ([^{3}H]-DPCPX) was purchased from PerkinElmer (Life and Analytical Sciences, Waltham, MA). Peptides for interfering with G protein signalling were obtained from Hello Bio (Bristol, UK) and were based on published sequences (Gilchrist et al., 2002). For G_{oa} the peptide had a sequence of MGIANNLRGCGLY. The scrambled version was LNRGNAYLCIGMG. For G_{ob} the peptide had a sequence of MGIQNNLKYIGIC. Peptides were made up as stock solutions (2 mM) and stored at -20°C. The stock solutions were dissolved in filtered intracellular solution just before use.

Molecular Dynamics Simulations

Ligand parameterization. The CHARMM36 (Huang and MacKerell, 2013; Huang et al., 2017)/CGenFF (Vanommeslaeghe and MacKerell, 2012; Vanommeslaeghe et al., 2012; Yu et al., 2012) force field combination was employed in all the molecular dynamic (MD) simulations performed. Initial topology and parameter files of BnOCPA, HOCPA, and PSB36 were obtained from the Paramchem webserver (Vanommeslaeghe and MacKerell, 2012). Higher penalties were associated with a few BnOCPA dihedral terms, which were therefore optimized at the HF/6-31G* level of theory using both the high throughput molecular dynamics (HTMD) (Doerr et al., 2016) parameterize functionality and the Visual Molecular Dynamics (VMD) (Humphrey et al., 1996) Force Field Toolkit (ffTK) (Mayne et al., 2013), after fragmentation of the molecule. Short MD simulations of BnOCPA in water were performed to visually inspect the behavior of the optimized rotatable bonds.

Systems preparation for fully dynamic docking of BnOCPA and HOCPA. Coordinates of the A_1R in the active, adenosine- and G protein-bound state were retrieved from the Protein Data Bank (Berman et al., 2003; Berman et al., 2000) database (PDB ID 6D9H (Draper-Joyce et al., 2018)). Intracellular loop 3 (ICL3) which is missing from PDB ID 6D9H was rebuilt using Modeller 9.19 (Fiser and Sali, 2003; Sali and Blundell, 1993). The G protein, with the exception of the C-terminal helix (helix 5) of the G protein alpha subunit (the key region responsible for the receptor TM6 active-like conformation) was removed from the system as in previous work (Dal Maso et al., 2018; Liang et al., 2018). BnOCPA and HOCPA were placed in the extracellular bulk, in two different systems, at least 20 Å from the receptor vestibule. The resulting systems were prepared for simulations using in-house scripts able to exploit both python HTMD (Doerr et al., 2016) and Tool Command Language (TCL) scripts. Briefly, this multistep procedure performs the preliminary hydrogen atoms addition by means of the pdb2pqr (Dolinsky et al., 2004) and propka (Olsson et al., 2011) software, considering a simulated pH of 7.0 (the proposed protonation of titratable side chains was checked by visual inspection). Receptors were then embedded in a square 80 Å x 80 Å 1-palmitoyl-2-oleyl-sn-glycerol-3-phosphocholine (POPC) bilayer (previously built by using the VMD Membrane Builder plugin 1.1, Membrane Plugin, Version 1.1.; http://www.ks.uiuc.edu/Research/vmd/plugins/membrane/) through an insertion method (Sommer, 2013), considering the A_1R coordinates retrieved from the OPM database (Lomize et al., 2006) to gain the correct orientation within the membrane. Lipids overlapping the receptor transmembrane bundle were removed and TIP3P water molecules (Jorgensen et al., 1983) were added to the simulation box (final dimensions 80 Å × 80 Å × 125 Å) using the VMD Solvate plugin 1.5 (Solvate Plugin, Version 1.5; http://www.ks.uiuc.edu/Research/vmd/plugins/solvate/). Finally, overall charge neutrality was achieved by adding Na^+/Cl^- counter ions (concentration of 0.150 M) using the VMD Autoionize plugin 1.3 (Autoionize Plugin, Version 1.3; http://www.ks.uiuc.edu/Research/vmd/plugins/autoionize/). All histidine side chains were considered in the delta tautomeric state, with the exception of H251 (epsilon tautomer) and H278 (protonated).

The MD engine ACEMD (Harvey et al., 2009) was employed for both the equilibration and productive simulations. Systems were equilibrated in isothermal-isobaric conditions (NPT) using the Berendsen

barostat (Berendsen et al., 1984) (target pressure 1 atm), the Langevin thermostat (Loncharich et al., 1992) (target temperature 300 K) with a low damping factor of 1 ps^{-1} and with an integration time step of 2 fs. Clashes between protein and lipid atoms were reduced through 2000 conjugate-gradient minimization steps before a 2 ns long MD simulation was run with a positional constraint of 1 kcal mol^{-1} $Å^{-2}$ on protein and lipid phosphorus atoms. Twenty nanoseconds of MD simulation were then performed constraining only the protein atoms. Lastly, positional constraints were applied only to the protein backbone alpha carbons for a further 5 ns.

Dynamic docking of BnOCPA and HOCPA. The supervised MD (SuMD) approach is an adaptive sampling method (Deganutti and Moro, 2017a) for simulating binding events in a timescale one or two orders of magnitudes faster than the corresponding classical (unsupervised) MD simulations (Sabbadin et al., 2018). SuMD has been successfully applied to small molecules and peptides (Cuzzolin et al., 2016; Deganutti et al., 2015; Deganutti and Moro, 2017b; Deganutti et al., 2018; Deganutti et al., 2017; Sabbadin and Moro, 2014; Salmaso et al., 2017). In the present work, the distances between the centers of mass of the adenine scaffold of the A_1R agonist and $N254^{6.55}$, $F171^{ECL2}$, $T277^{7.42}$ and $H278^{7.43}$ of the receptor were considered for the supervision during the MD simulations. The dynamic docking of BnOCPA was hindered by the ionic bridge formed between the $E172^{ECL2}$ and $K265^{ECL3}$ side chains. A metadynamics (Branduardi et al., 2007; Laio and Parrinello, 2002; Laio et al., 2005) energetic bias was therefore introduced in order to facilitate the rupture of this ionic interaction, thus favoring the formation of a bound complex. More precisely, Gaussian terms (height = 0.01 kcal mol^{-1} and widths = 0.1 Å) were deposited every 1 ps along the distance between the $E172^{ECL2}$ carboxyl carbon and the positively charged $K265^{ECL3}$ nitrogen atom using PLUMED 2.3 (Tribello et al., 2014). A similar SuMD-metadynamics hybrid approach was previously employed to study binding/unbinding kinetics (Deganutti et al., 2016) on the $A_{2A}R$ subtype. For each replica (Methods Table 1), when the ligands reached a bound pose (i.e. a distance between the adenine and the receptor residues centers of mass < 3 Å), a classic (unsupervised and without energetic bias) MD simulation was performed for at least a further 100 ns.

BnOCPA bound state metadynamics. We decided to perform a detailed analysis of the role played by the $E172^{ECL2}$ - $K265^{ECL3}$ ionic interaction in the dynamic docking of BnOCPA. Three 250 ns long

well-tempered (Barducci et al., 2008) metadynamics simulations were performed using the bound state obtained from a previous dynamic docking simulation, which resulted in binding mode A, as a starting point. The collective variables (CVs) considered were: i) the distance between the $E172^{ECL2}$ carboxyl carbon and the positively charged $K265^{ECL3}$ nitrogen atom and ii) the dihedral angle formed by the 4 atoms linking the cyclopentyl ring to the phenyl moiety (which was the most flexible ligand torsion during the previous SuMD simulations). Gaussian widths were set at 0.1 Å and 0.01 radians respectively, heights at 0.01 kcal/mol^{-1}, and the deposition was performed every 1 ps (bias-factor = 5). Although complete convergence was probably not reached, three replicas (Methods Table 1) allowed sampling of three main energetic minima on the energy surface (Figure S6); these correspond to the representative binding poses shown in Figure 3D to F.

Classic MD simulations of BnOCPA binding modes A, B, C and D. To test the hypothesis that BnOCPA and HOCPA may differently affect TM6 and/or TM7 mobility when bound to A_1R (and to further sample the stability of each BnOCPA binding mode), putative binding conformations A, B and C (Figure 3) were superposed to the experimental A_1R active state coordinates with the modelled ICL3. This should have removed any A_1R structural artefacts, possibly introduced by metadynamics. As reference and control, two further systems were considered: i) the pseudo-apo A_1R and ii) the selective A_1R antagonist PSB36 (Cheng et al., 2017) superposed in the same receptor active conformation (Methods Table 1). The BnOCPA binding mode D was modelled from mode B by rotating the dihedral angle connecting the cyclopentyl ring and the N6 nitrogen atom in order to point the benzyl of the agonist toward the hydrophobic pocket underneath ECL3 (Figure 3G) delimited by $L253^{6.56}$, $T257^{6.52}$, $K265^{ECL3}$,$T270^{7.35}$, and $L269^{7.34}$. The G protein atoms were removed, and the resulting systems prepared for MD as reported above. A similar comparison was performed in a milestone study on the β_2 adrenergic receptor (Dror et al., 2011) which sought to describe the putative deactivation mechanism of the receptor.

Dynamic docking of the Goa, Gob and Gi2 GαCT helix. A randomly extracted frame from the classic MD performed on the BnOCPA:A1R complex was prepared for three sets of simulations placing the GαCT helix 5 (last 27 residues) of the Gα proteins Goa, Gob and Gi2 in the intracellular solvent bulk side of the simulation boxes. As a further control, a frame from the classic MD performed

on the unbiased ligand HOCPA:A_1R complex was randomly extracted and prepared along with the Gob GαCT. The resulting four systems were embedded in a POPC membrane and prepared as reported above.

The different structural effects putatively triggered by BnOCPA and HOCPA on the recognition mechanism of Goa, Gob and Gi2 GαCT were studied by performing 10 SuMD replicas (Methods Table 1). During each replica (Video S3), the distance between the centroid of the GαCT residues 348-352 and the centroid of the A1R residues D42$^{2.37}$, I232$^{6.33}$, and Q293$^{8.48}$ was supervised until it reached a value lower than 8 Å. A classic MD simulation was then run for a further 300 ns.

Classic MD simulations on the A_1R:Goa and Gob complexes. The A_1R cryo-EM structure (PDB ID 6D9H) was used as template for all the five systems simulated (Methods Table 1). The endogenous agonist adenosine was removed and HOCPA and BnOCPA (modes B and D) were inserted in the orthosteric site superimposing 6D9H to the systems prepared for the classic MD simulations in the absence of G protein. ICL3 was not modelled, nor were the missing part of the G protein α subunit. As subunits β and γ were removed, the Gα NT helix was truncated to residue 27 to avoid unnatural movements (NT is constrained by Gβ in 6D9H). The Gα subunit was mutated according to the Goa and Gob primary sequences (Jiang and Bajpayee, 2009) using in-house scripts. The resulting five systems (Methods Table 1) were embedded in a POPC membrane and prepared as reported above.

Analysis of the classic MD simulations. During the classic MD simulations that started from Modes A-C (Figure 3D to F), BnOCPA had the tendency to explore the three conformations by rapidly interchanging between the three binding modes. In order to determine the effect exerted on the TM domain by each conformation, 21 μs of MD simulations (Methods Table 1 - BnOCPA mode A, BnOCPA mode B, BnOCPA mode C) were subjected to a geometric clustering. More precisely, a simulation frame was considered in pose A if the distance between the phenyl ring of BnOCPA and the I175^{ECL2} alpha carbon was less than 5 Å; in pose B if the distance between the phenyl ring of BnOCPA and the L258$^{6.59}$ alpha carbon was less than 6 Å, and in pose C if the distance between the phenyl ring of BnOCPA and the Y271$^{7.36}$ alpha carbon was less than 6 Å. During the MD

simulations started from mode D (Figure 3G), a frame was still considered in mode D if the root mean square deviation (RMSD) of the benzyl ring to the starting equilibrated conformation was less than 3 Å. For each of the resulting four clusters, the RMSD of the GPCR conserved motif NPXXY ($N^{7.49}$ PIV $Y^{7.53}$ in the A_1R; Figure S7) was computed using Plumed 2.3 (Tribello et al., 2014) considering the inactive receptor state as reference, plotting the obtained values as frequency distributions (Figure 3I, J). Rearrangement of the NPXXY motif, which is located at the intracellular half of TM7, is considered one of the structural hallmarks of GPCR activation (Rosenbaum et al., 2009). Upon G protein binding, it moves towards the center of the receptor TM bundle (Figure S7). Unlike other activation micro-switches (e.g. the break/formation of the salt bridge between $R^{3.50}$ and $E^{6.30}$), this conformational transition is believed to occur in timescales accessible to MD simulations (Dror et al., 2011).

Hydrogen bonds and atomic contacts were computed using the GetContacts analysis tool (https://github.com/getcontacts/getcontacts) and expressed in terms of occupancy (the percentage of MD frames in which the interaction occurred).

Analysis of the Goa, Gob and Gi2 GαCT classic MD simulations after SuMD. For each system, only the classic MD simulations performed after the GαCT reached the A1R intracellular binding site were considered for the analysis.

The RMSD values to the last 15 residues of the Gi2 GαCT reported in the A_1R cryo-EM PDB structure 6D9H were computed using VMD (Humphrey et al., 1996). The MD frames associated with the peaks in the RMSD plots (states CS1, MS1, MS2 and MS3 in Figure 4A, D) were clustered employing the VMD Clustering plugin (https://github.com/luisico/clustering) by selecting the whole GαCT helixes alpha carbon atoms and a cutoff of 3 Å.

Methods Table 1. Summary of the simulations performed.

Ligand	MD approach	# Replicas	Total simulated time[a]
BnOCPA	SuMD	6	1.9 μs
BnOCPA	SuMD-Metadynamics	5	4.3 μs
HOCPA	SuMD	5	3.4 μs
BnOCPA (bound state after dynamic docking)	Metadynamics	3	0.75 μs
BnOCPA(A)	Classic MD	6	9.0 μs
BnOCPA(B)	Classic MD	6	9.0 μs
BnOCPA(C)	Classic MD	3	3.0 μs
HOCPA	Classic MD	4	8.0 μs
PSB36	Classic MD	4	6.0 μs
Apo A_1	Classic MD	4	8.0 μs
GαCT Goa (BnOCPA)	SuMD + Classic MD	10	0.36 μs + 3.0 μs
GαCT Gob (BnOCPA)	SuMD + Classic MD	10	0.33 μs + 3.0 μs
GαCT Gi2 (BnOCPA)	SuMD + Classic MD	10	0.37 μs + 3.0 μs
GαCT Gob (HOCPA)	SuMD + Classic MD	10	0.29 μs + 3.0 μs
BnOCPA(D):Gob	Classic MD	4	4.0 μs
BnOCPA(B):Gob	Classic MD	3	3.0 μs
HOCPA:Gob	Classic MD	4	4.0 μs
BnOCPA(D):Goa	Classic MD	5	5.0 μs
BnOCPA(B):Goa	Classic MD	4	4.0 μs

a) For SuMD and SuMD-metadynamics simulations the time is the sum of productive SuMD time windows.

(A), (B), (C) and (D) indicate the respective BnOCPA binding modes.

Related to Figure 3.

Methods References

Anderson, W.W., and Collingridge, G.L. (2007). Capabilities of the WinLTP data acquisition program extending beyond basic LTP experimental functions. JNeurosciMethods *162*, 346-356.

Barducci, A., Bussi, G., and Parrinello, M. (2008). Well-tempered metadynamics: a smoothly converging and tunable free-energy method. Phys Rev Lett *100*, 020603.

Barkan, K., Lagarias, P., Vrontaki, E., Stamatis, D., Hoare, S., Klotz, K.-N., Kolocouris, A., and Ladds, G. (2019). Pharmacological Characterisation of Novel Adenosine Receptor A3R Antagonists. bioRxiv, 693796.

Berendsen, H.J.C., Postma, J.P.M., van Gunsteren, W.F., DiNola, A., and Haak, J.R. (1984). Molecular dynamics with coupling to an external bath. J Chem Phys *81*, 3684.

Berman, H., Henrick, K., and Nakamura, H. (2003). Announcing the worldwide Protein Data Bank. Nat Struct Biol *10*, 980.

Berman, H.M., Westbrook, J., Feng, Z., Gilliland, G., Bhat, T.N., Weissig, H., Shindyalov, I.N., and Bourne, P.E. (2000). The Protein Data Bank. Nucleic Acids Res *28*, 235-242.

Black, J.W., and Leff, P. (1983). Operational models of pharmacological agonism. Proc R Soc Lond B Biol Sci *220*, 141-162.

Branduardi, D., Gervasio, F.L., and Parrinello, M. (2007). From A to B in free energy space. J Chem Phys *126*, 054103.

Cheng, R.K.Y., Segala, E., Robertson, N., Deflorian, F., Doré, A.S., Errey, J.C., Fiez-Vandal, C., Marshall, F.H., and Cooke, R.M. (2017). Structures of Human A1 and A2A Adenosine Receptors with Xanthines Reveal Determinants of Selectivity. Structure *25*, 1275-1285.e1274.

Cheng, Y., and Prusoff, W.H. (1973). Relationship between the inhibition constant (K1) and the concentration of inhibitor which causes 50 per cent inhibition (I50) of an enzymatic reaction. Biochem Pharmacol *22*, 3099-3108.

Cuzzolin, A., Sturlese, M., Deganutti, G., Salmaso, V., Sabbadin, D., Ciancetta, A., and Moro, S. (2016). Deciphering the Complexity of Ligand-Protein Recognition Pathways Using Supervised Molecular Dynamics (SuMD) Simulations. J Chem Inf Model *56*, 687-705.

Dal Maso, E., Zhu, Y., Pham, V., Reynolds, C.A., Deganutti, G., Hick, C.A., Yang, D., Christopoulos, A., Hay, D.L., Wang, M.-W.*, et al.* (2018). Extracellular loops 2 and 3 of the calcitonin receptor selectively modify agonist binding and efficacy. Biochemical Pharmacology *150*, 214-244.

Deganutti, G., Cuzzolin, A., Ciancetta, A., and Moro, S. (2015). Understanding allosteric interactions in G protein-coupled receptors using Supervised Molecular Dynamics: A prototype study analysing

the human A3 adenosine receptor positive allosteric modulator LUF6000. Bioorg Med Chem *23*, 4065-4071.

Deganutti, G., and Moro, S. (2017a). Estimation of kinetic and thermodynamic ligand-binding parameters using computational strategies. Future Med Chem *9*, 507-523.

Deganutti, G., and Moro, S. (2017b). Supporting the Identification of Novel Fragment-Based Positive Allosteric Modulators Using a Supervised Molecular Dynamics Approach: A Retrospective Analysis Considering the Human A2A Adenosine Receptor as a Key Example. Molecules *22*.

Deganutti, G., Salmaso, V., and Moro, S. (2018). Could Adenosine Recognize its Receptors with a Stoichiometry Other than 1 : 1? Mol Inform *37*.

Deganutti, G., Welihinda, A., and Moro, S. (2017). Comparison of the Human A2A Adenosine Receptor Recognition by Adenosine and Inosine: New Insight from Supervised Molecular Dynamics Simulations. ChemMedChem *12*, 1319-1326.

Deganutti, G., Zhukov, A., Deflorian, F., Federico, S., Spalluto, G., Cooke, R.M., Moro, S., Mason, J.S., and Bortolato, A. (2016). Impact of protein–ligand solvation and desolvation on transition state thermodynamic properties of adenosine A2A ligand binding kinetics. In Silico Pharmacol *5*, 16.

Doerr, S., Harvey, M.J., Noé, F., and De Fabritiis, G. (2016). HTMD: High-Throughput Molecular Dynamics for Molecular Discovery. J Chem Theory Comput *12*, 1845-1852.

Dolinsky, T.J., Nielsen, J.E., McCammon, J.A., and Baker, N.A. (2004). PDB2PQR: an automated pipeline for the setup of Poisson-Boltzmann electrostatics calculations. Nucleic Acids Res *32*, W665-667.

Draper-Joyce, C.J., Khoshouei, M., Thal, D.M., Liang, Y.-L., Nguyen, A.T.N., Furness, S.G.B., Venugopal, H., Baltos, J.-A., Plitzko, J.M., Danev, R.*, et al.* (2018). Structure of the adenosine-bound human adenosine A1 receptor-Gi complex. Nature *558*, 559-563.

Dror, R.O., Arlow, D.H., Maragakis, P., Mildorf, T.J., Pan, A.C., Xu, H., Borhani, D.W., and Shaw, D.E. (2011). Activation mechanism of the β2-adrenergic receptor. Proc Natl Acad Sci USA *108*, 18684-18689.

Evans, B. (1989). Adenosine Derivatives, E.P. Office, ed.

Fiser, A., and Sali, A. (2003). Modeller: generation and refinement of homology-based protein structure models. Meth Enzymol *374*, 461-491.

Frenguelli, B.G., and Wall, M.J. (2016). Combined electrophysiological and biosensor approaches to study purinergic regulation of epileptiform activity in cortical tissue. J Neurosci Methods *260*, 202-214.

Gilchrist, A., Li, A., and Hamm, H.E. (2002). G alpha COOH-terminal minigene vectors dissect heterotrimeric G protein signaling. Sci STKE *2002*, pl1.

Harvey, M.J., Giupponi, G., and Fabritiis, G.D. (2009). ACEMD: Accelerating Biomolecular Dynamics in the Microsecond Time Scale. J Chem Theory Comput *5*, 1632-1639.

Huang, J., and MacKerell, A.D. (2013). CHARMM36 all-atom additive protein force field: validation based on comparison to NMR data. J Comput Chem *34*, 2135-2145.

Huang, J., Rauscher, S., Nawrocki, G., Ran, T., Feig, M., de Groot, B.L., Grubmüller, H., and MacKerell, A.D. (2017). CHARMM36m: an improved force field for folded and intrinsically disordered proteins. Nat Methods *14*, 71-73.

Humphrey, W., Dalke, A., and Schulten, K. (1996). VMD: visual molecular dynamics. J Mol Graph *14*, 33-38, 27-38.

Jagtap, P. (2011). Adenosine compounds and their use thereof. In WO2011/119919 A1, W.I.P. Organization, ed., pp. WO2011/119919 A119911.

Jiang, M., and Bajpayee, N.S. (2009). Molecular mechanisms of Go signaling. Neurosignals *17*, 23-41.

Jorgensen, W.L., Chandrasekhar, J., Madura, J.D., Impey, R.W., and Klein, M.L. (1983). Comparison of simple potential functions for simulating liquid water. J Chem Phys *79*, 926.

Kim, S.H., and Chung, J.M. (1992). An experimental model for peripheral neuropathy produced by segmental spinal nerve ligation in the rat. Pain *50*, 355-363.

Knight, A., Hemmings, J.L., Winfield, I., Leuenberger, M., Frattini, E., Frenguelli, B.G., Dowell, S.J., Lochner, M., and Ladds, G. (2016). Discovery of novel adenosine receptor agonists that exhibit subtype selectivity. J Med Chem *59*, 947-964.

Laio, A., and Parrinello, M. (2002). Escaping free-energy minima. Proc Natl Acad Sci USA *99*, 12562-12566.

Laio, A., Rodriguez-Fortea, A., Gervasio, F.L., Ceccarelli, M., and Parrinello, M. (2005). Assessing the accuracy of metadynamics. J Phys Chem B *109*, 6714-6721.

Liang, Y.-L., Khoshouei, M., Deganutti, G., Glukhova, A., Koole, C., Peat, T.S., Radjainia, M., Plitzko, J.M., Baumeister, W., Miller, L.J.*, et al.* (2018). Cryo-EM structure of the active, Gs-protein complexed, human CGRP receptor. Nature *561*, 492-497.

Lomize, M.A., Lomize, A.L., Pogozheva, I.D., and Mosberg, H.I. (2006). OPM: orientations of proteins in membranes database. Bioinformatics *22*, 623-625.

Loncharich, R.J., Brooks, B.R., and Pastor, R.W. (1992). Langevin dynamics of peptides: the frictional dependence of isomerization rates of N-acetylalanyl-N'-methylamide. Biopolymers *32*, 523-535.

Mayne, C.G., Saam, J., Schulten, K., Tajkhorshid, E., and Gumbart, J.C. (2013). Rapid parameterization of small molecules using the Force Field Toolkit. J Comput Chem *34*, 2757-2770.

Olsson, M.H.M., Søndergaard, C.R., Rostkowski, M., and Jensen, J.H. (2011). PROPKA3: Consistent Treatment of Internal and Surface Residues in Empirical pK Predictions. J Chem Theory Comput *7*, 525-537.

Rosenbaum, D.M., Rasmussen, S.G., and Kobilka, B.K. (2009). The structure and function of G-protein-coupled receptors. Nature *459*, 356-363.

Sabbadin, D., and Moro, S. (2014). Supervised molecular dynamics (SuMD) as a helpful tool to depict GPCR-ligand recognition pathway in a nanosecond time scale. J Chem Inf Model *54*, 372-376.

Sabbadin, D., Salmaso, V., Sturlese, M., and Moro, S. (2018). Supervised molecular dynamics (sumd) approaches in drug design, Vol 1824.

Sali, A., and Blundell, T.L. (1993). Comparative protein modelling by satisfaction of spatial restraints. J Mol Biol *234*, 779-815.

Salmaso, V., Sturlese, M., Cuzzolin, A., and Moro, S. (2017). Exploring Protein-Peptide Recognition Pathways Using a Supervised Molecular Dynamics Approach. Structure *25*, 655-662.e652.

Sommer, B. (2013). Membrane Packing Problems: A short Review on computational Membrane Modeling Methods and Tools. Comput Struct Biotechnol J *5*, e201302014.

Stoddart, L.A., Johnstone, E.K.M., Wheal, A.J., Goulding, J., Robers, M.B., Machleidt, T., Wood, K.V., Hill, S.J., and Pfleger, K.D.G. (2015). Application of BRET to monitor ligand binding to GPCRs. Nat Methods *12*, 661-663.

Stoddart, L.A., Vernall, A.J., Denman, J.L., Briddon, S.J., Kellam, B., and Hill, S.J. (2012). Fragment screening at adenosine-A(3) receptors in living cells using a fluorescence-based binding assay. Chem Biol *19*, 1105-1115.

Strong, P., Anderson, R., Coates, J., Ellis, F., Evans, B., Gurden, M.F., Johnstone, J., Kennedy, I., and Martin, D.P. (1993). Suppression of non-esterified fatty acids and triacylglycerol in experimental animals by the adenosine analogue GR79236. Clin Sci (Lond) *84*, 663-669.

Tribello, G.A., Bonomi, M., Branduardi, D., Camilloni, C., and Bussi, G. (2014). PLUMED 2: New feathers for an old bird. Comput Phys Commun *185*, 604-613.

Vanommeslaeghe, K., and MacKerell, A.D., Jr. (2012). Automation of the CHARMM General Force Field (CGenFF) I: bond perception and atom typing. J Chem Inf Model *52*, 3144-3154.

Vanommeslaeghe, K., Raman, E.P., and MacKerell, A.D. (2012). Automation of the CHARMM General Force Field (CGenFF) II: assignment of bonded parameters and partial atomic charges. J Chem Inf Model *52*, 3155-3168.

Vernall, A.J., Stoddart, L.A., Briddon, S.J., Hill, S.J., and Kellam, B. (2012). Highly potent and selective fluorescent antagonists of the human adenosine A(3) receptor based on the 1,2,4-triazolo[4,3-a]quinoxalin-1-one scaffold. J Med Chem *55*, 1771-1782.

Wall, M.J., and Dale, N. (2013). Neuronal transporter and astrocytic ATP exocytosis underlie activity-dependent adenosine release in the hippocampus. JPhysiol *591*, 3853-3871.

Weston, C., Winfield, I., Harris, M., Hodgson, R., Shah, A., Dowell, S.J., Mobarec, J.C., Woodcock, D.A., Reynolds, C.A., Poyner, D.R.*, et al.* (2016). Receptor activity-modifying protein-directed G protein signaling specificity for the calcitonin gene-related peptide family of receptors. J Biol Chem *291*, 25763.

Yu, W., He, X., Vanommeslaeghe, K., and MacKerell, A.D. (2012). Extension of the CHARMM General Force Field to sulfonyl-containing compounds and its utility in biomolecular simulations. J Comput Chem *33*, 2451-2468.